

RESEARCH ARTICLE

Schwann cell reprogramming into repair cells increases miRNA-21 expression in exosomes promoting axonal growth

Rodrigo López-Leal^{1,2}, Florencia Díaz-Viraqué³, Romina J. Catalán^{1,2}, Cristian Saquel^{1,2}, Anton Enright⁴, Gregorio Iraola^{1,5} and Felipe A. Court^{1,2,6,*}

ABSTRACT

Functional recovery after peripheral nerve damage is dependent on the reprogramming of differentiated Schwann cells (dSCs) into repair Schwann cells (rSCs), which promotes axonal regeneration and tissue homeostasis. Transition into a repair phenotype requires expression of c-Jun and Sox2, which transcriptionally mediates inhibition of the dSC program of myelination and activates a non-cell-autonomous repair program, characterized by the secretion of neuronal survival and regenerative molecules, formation of a cellular scaffold to guide regenerating axons and activation of an innate immune response. Moreover, rSCs release exosomes that are internalized by peripheral neurons, promoting axonal regeneration. Here, we demonstrate that reprogramming of Schwann cells (SCs) is accompanied by a shift in the capacity of their secreted exosomes to promote neurite growth, which is dependent on the expression of c-Jun (also known as Jun) and Sox2 by rSCs. Furthermore, increased expression of miRNA-21 is responsible for the pro-regenerative capacity of rSC exosomes, which is associated with PTEN downregulation and PI3-kinase activation in neurons. We propose that modification of exosomal cargo constitutes another important feature of the repair program of SCs, contributing to axonal regeneration and functional recovery after nerve injury.

KEY WORDS: Schwann cell, Exosomes, Axonal outgrowth, Axonal regeneration, miRNA-21

INTRODUCTION


Regeneration of injured peripheral nerve axons is critically dependent on the response of Schwann cells (SCs) to nerve injury. This dependency on glial cells for efficient axonal regeneration and functional recovery is associated with the reprogramming of differentiated Schwann cells (dSCs) into a cell phenotype, known as a repair Schwann cell (rSC), that is specialized for promoting regeneration and tissue homeostasis. Features of rSCs critical for promoting functional recovery after nerve damage include (i) secretion of neuronal survival and pro-regenerative

molecules (Boyd and Gordon, 2003; Wood and Mackinnon, 2015), (ii) formation of a cellular scaffold to guide regenerating axons, including the expression of adhesive molecules and the molecular remodeling of basal laminae (Gardiner, 2011; Jessen and Mirsky, 2016), (iii) downregulation of myelin components and elimination of myelin remnants by a process known as myelinophagy (Gomez-Sanchez et al., 2015) and (iv) mounting an innate immune response, involving macrophage recruitment for clearing axonal and myelin debris (Chen et al., 2015; Martini et al., 2008; Shamash et al., 2002). This adaptive SC reprogramming (Jessen et al., 2015; Jessen and Arthur-Farraj, 2019), which leads to the loss of myelin differentiation and activation of a repair program, depends on the activation of transcriptional mechanisms different from those associated with SC differentiation during development (Arthur-Farraj et al., 2017; Clements et al., 2017). Transition to the rSC phenotype involves several transcriptional regulators, including c-Jun (also known as Jun), Sox2, merlin (Nf2), Stat3, and chromatin remodeling (Mindos et al., 2017). The transcription factor c-Jun is upregulated in SCs upon nerve injury and is responsible for inhibiting myelination and activation of the abovementioned repair program (Parkinson et al., 2008; Arthur-Farraj et al., 2012), whereas Sox2 acts as a negative regulator of myelination in rSCs and also drives changes that promote axonal regeneration. Indeed, decreased c-Jun expression by genetic targeting is associated with slower axonal regeneration and functional recovery after nerve injury (Parkinson et al., 2008), whereas its overexpression enhances axonal degeneration in poor regenerative settings such as advanced age and chronic denervation (Fazal et al., 2017). Sox2, in turn, is involved in activating an inflammatory response after nerve damage (Roberts et al., 2017). Indeed, overexpression of Sox2 enhances SC proliferation and increases macrophage infiltration in undamaged nerves (Roberts et al., 2017).

Therefore, reprogramming of SCs to the repair phenotype involves known molecular regulators that generate a specialized cell for successful axonal regeneration, leading to morphological modifications and profound changes in molecular programs. We have previously shown that rSCs release exosomes that are internalized by peripheral neurons and that strongly enhance neurite growth and axonal regeneration *in vitro* and *in vivo*, respectively (Lopez-Verrilli et al., 2013). Exosomes are nano-sized extracellular vesicles generated in the endosomal compartment and loaded with different cargo molecules including RNA species and proteins. It has been demonstrated that exosomes can profoundly modulate diverse cellular processes in a non-cell-autonomous fashion, including cellular migration, differentiation and response to tissue damage (van Niel et al., 2018; Steenbeek et al., 2018). After the initial demonstration of a pro-regenerative role for glial exosomes (Lopez-Verrilli et al., 2013; Lopez-Leal and Court, 2016), it has been shown that exosome-mediated mobilization of non-coding RNA and proteins to neurons promotes neurite outgrowth and axonal regeneration in the peripheral and central

¹Center for Integrative Biology, Faculty of Sciences, Universidad Mayor, Santiago 8580745, Chile. ²Fondap Geroscience Center for Brain Health and Metabolism, Santiago 7800003, Chile. ³Laboratorio de Interacciones Hospedero Patógeno – Unidad de Biología Molecular, Institut de Pasteur Montevideo, Mataojo 2020, Montevideo 11400, Uruguay. ⁴Department of Pathology, University of Cambridge, Cambridge CB2 1QP, UK. ⁵Microbial Genomics Laboratory, Institut Pasteur de Montevideo, Mataojo 2020, Montevideo 11400, Uruguay. ⁶Buck Institute for Research on Aging, Novato, CA 94945, USA.

*Author for correspondence (felipe.court@umayor.cl)

 R.L.-L., 0000-0003-2153-0193; F.D.-V., 0000-0003-0181-3671; R.J.C., 0000-0002-3467-3516; C.S., 0000-0002-9809-4556; F.A.C., 0000-0002-9394-7601

Handling Editor: Giampietro Schiavo
Received 6 September 2019; Accepted 24 April 2020

nervous systems (Holm et al., 2018; Rajendran et al., 2014; Tasew et al., 2017; Huang et al., 2018; Hervera et al., 2018).

Although the effect of cell-derived exosomes in cellular reprogramming has been demonstrated in physiological and pathological conditions (McNamara et al., 2019; La Shu et al., 2018), whether cell reprogramming impacts the content, and therefore the biological activity, of the secreted exosomes has not been explored. Here, we investigated whether the adaptive cellular reprogramming of dSCs into rSCs is accompanied by a shift in the capacity of their secreted exosomes to promote neurite growth. Our data demonstrate that the capacity of SC exosomes to stimulate neurite growth is restricted to those secreted by rSCs. Furthermore, this enhancement of growth by rSC-derived exosomes is dependent on rSC expression of c-Jun and Sox2, key transcription factors of the SC repair program. Indeed, HEK cell-derived exosomes strongly promote neurite growth after forced expression of human c-Jun or SOX2. Mechanistically, the shift of SC-derived exosomes to this phenotype that enhances neurite growth is dependent on the increased expression of miRNA-21 by rSC-derived exosomes and is associated with downregulation of the miRNA-21 target gene *PTEN* and PI3-kinase (PI3K) activation. Our results demonstrate that cellular reprogramming of SCs into the repair phenotype involves a modification in their exosome miRNA cargo and their effects on neurite growth. We propose that modification of exosomal cargo constitutes another important feature of the repair program of SCs, contributing to axonal regeneration and functional recovery after nerve injury.

RESULTS

Pharmacological modulation of the SC phenotype *in vitro*

Exosomes derived from rSCs enhance neurite growth and axonal regeneration *in vitro* and *in vivo* (Lopez-Verrilli et al., 2013). Nevertheless, whether the effects of secreted exosomes are specifically associated with the rSC phenotype is currently unknown. In order to explore this idea, we first implemented a reliable *in vitro* method to culture SCs in a way that led them to adopt either the differentiated or repair phenotype. To this end, we adapted a protocol based on the differential effects of cyclic-AMP (cAMP) levels on the phenotype of SCs (Monje et al., 2009). Primary cultures of SCs from rat neonates cultured in the presence of the cAMP analogs dibutyl-AMP (db-cAMP) or 8-(4-chlorophenylthio)-cAMP (cpt-cAMP) showed key molecular signatures of dSCs, including high expression of the myelin protein MBP and low expression of the transcription factors c-Jun and Sox2 (Fig. 1A), which contrasted with SCs cultured in a low concentration of forskolin (Fsk2), which were negative for MBP expression but expressed high levels of c-Jun and Sox2 (Fig. 1A,B). In addition, the proliferative capacity of SCs treated with Fsk2 was double that of SCs treated with either db-cAMP or cpt-cAMP (Fig. 1A–C), which indicated that the Fsk2-treated SCs had reprogrammed into a repair phenotype. Finally, reverse transcription quantitative PCR (RT-qPCR) was used to test bona fide markers of each SC state. Relative to cells treated with Fsk2, cells treated with the cAMP analogs expressed lower levels of the rSC markers *Sox2*, *Lif*, *Artn* (which encodes artemin) and *Bdnf*, and high levels of *Mbp* mRNA (Fig. 1D). Taken together, these data show that SCs *in vitro* can be pharmacologically modulated to express a differentiated or repair-like phenotype.

Exosomes derived from rSCs, but not from dSCs, enhance neurite growth

We next tested whether the SC phenotype was associated with the capacities of their derived exosomes to enhance neurite growth. To

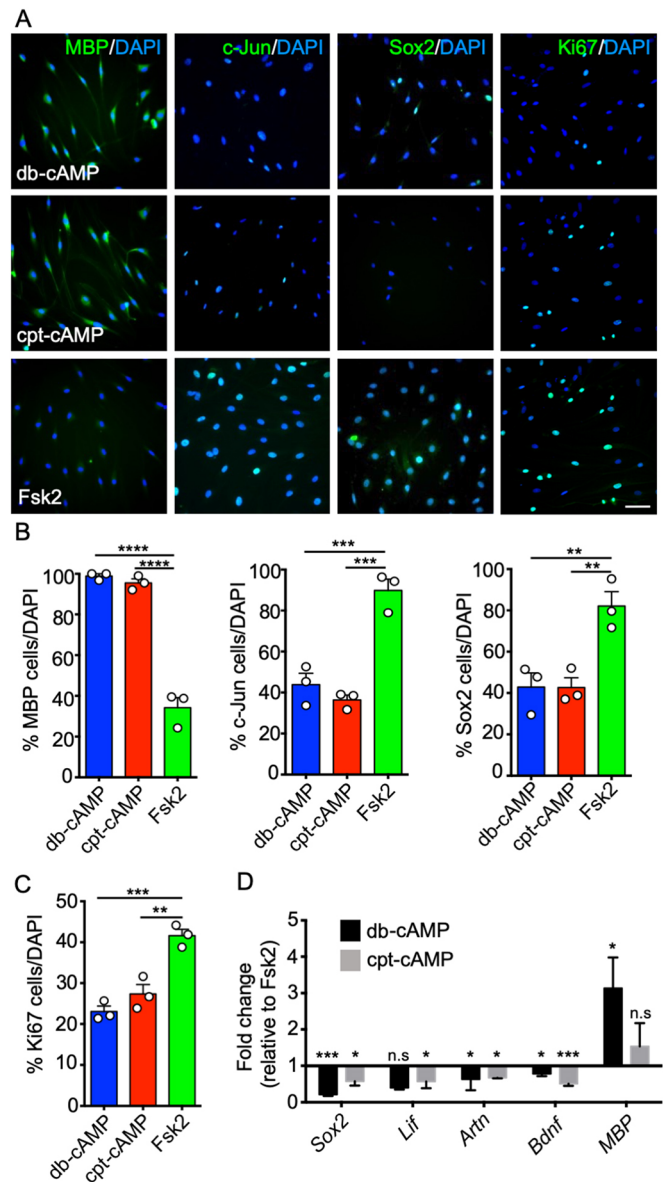


Fig. 1. Schwann cell reprogramming *in vitro* by pharmacological treatment.

(A) IF of SC cultures stained for c-Jun, Sox2, MBP or Ki67 (also known as Mki67) (green), together with DAPI (blue) to stain nuclei. SCs were treated for 5 d with 2 μ M forskolin (Fsk2), 1 mM db-cAMP or 250 μ M cpt-cAMP. Scale bar: 50 μ m. (B) IF quantification of total cells positive for the SC markers (green in A) compared to the total cell number as determined by nuclear DAPI staining (blue in A). Fifty cells per field were quantified in three fields per condition. $n=3$ per treatment from three separate experiments. (C) Proliferation analysis was performed using Ki67 immunostaining after 5 d treatment with 2 μ M forskolin (Fsk2), 1 mM db-cAMP or 250 μ M cpt-cAMP. The number of Ki67-positive cells (green in A) were compared to the total cell number by nuclear DAPI staining (blue in A). Fifty cells per field were quantified in three fields per condition. $n=3$ per treatment from three separate experiments. (D) RT-qPCR from SC mRNA preparations. SCs were treated for 5 d with 2 μ M forskolin (Fsk2), 1 mM db-cAMP or 250 μ M cpt-cAMP. The quantification of PCR products was performed using the $2^{-\Delta\Delta C_t}$ method, and the quantity of mRNA was normalized to the housekeeping gene *Gapdh*. The assays were performed in triplicate. Data shown are mean \pm s.e.m. * $P<0.05$; ** $P<0.001$; *** $P<0.0005$; **** $P<0.00001$; n.s., not significant (ANOVA test followed by Bonferroni post-test).

this end, exosomes were purified by differential ultracentrifugation from the conditioned medium of SCs cultured in the presence of Fsk2 or the cAMP analogs db-cAMP and cpt-cAMP. Importantly,

SCs in these different culture conditions secrete a comparable number of exosomes, and the exosome size profile was similar when analyzed by Nanosight nanoparticle tracking (Fig. S1A,B). Next, neurite growth of sensory neurons was evaluated in dorsal root ganglia (DRG) explants in the presence of equal amounts of exosomes purified from SCs exposed to Fsk2, db-cAMP or cpt-cAMP (120 ng/ml; see Table S1). As expected, exosomes derived from rSCs strongly enhanced neurite growth by a factor of two when compared to neurite growth of vehicle-treated neurons (Fig. 2A,B). Nevertheless, exosomes derived from dSCs failed to enhance neurite growth (Fig. 2A,B). Importantly, the enhancement of neurite outgrowth by rSC exosomes was not observed when rSC-conditioned medium devoid of exosomes was added to DRG neurons (Fig. S2A,B), suggesting that under NGF-supplemented conditions, neurite growth cannot be further activated by paracrine factors derived from rSCs. We next evaluated whether exosomes derived from dSCs or rSCs were similarly internalized by sensory neurons. For this, SCs expressing palmitoylated eGFP (palm-eGFP), which is strongly expressed in exosomes (Lai et al., 2015),

were treated with either Fsk2 or cpt-cAMP. Then, DRG neurons were exposed to the same number of exosomes purified from palm-eGFP-expressing SCs. After 3 h, similar amounts of GFP-expressing exosomes derived from Fsk2- or cpt-cAMP-treated SCs were detected in neurites and growth cones of sensory neurons (Fig. 2C,D), demonstrating that the contrasting effects of dSC- and rSC-derived exosomes on neurite outgrowth is not due to differences in exosome internalization by sensory neurons, and suggesting that changes in exosomal content might be associated with this effect.

Expression of c-Jun and Sox2 modulates the effect of exosomes on neurite growth

Because expression of c-Jun and Sox2 are involved in the adaptive cellular reprogramming of dSCs into rSCs, we used a genetic strategy in order to define whether the capacity of rSC-derived exosomes to enhance neurite growth was dependent on these transcription factors. To this end, c-Jun or Sox2 were downregulated in rSCs (cultured in Fsk2) using shRNA co-expressing eGFP to identify transfected SCs (Fig. 3A). Compared to scrambled shRNA, c-Jun and Sox2 shRNAs effectively downregulated nuclear expression of the corresponding protein in eGFP-expressing SCs (Fig. 3A,B). We next purified exosomes from these shRNA-transfected rSC cultures and tested their capacity to promote neurite growth. Compared to exosomes derived from control rSC cultures (scramble shRNA), neurite extension was significantly reduced when neurons were treated with exosomes derived from rSCs expressing either c-Jun or Sox2 shRNAs (Fig. 3C, D). Because exosomes derived from rSCs promoted axonal growth in a c-Jun- and Sox2-dependent manner, we examined whether the expression of these transcription factors was sufficient to generate exosomes that enhance neurite growth. To this end, we used HEK293 (HEK) cells, which secrete exosomes without neurite pro-growth capacities (Tassew et al., 2017). HEK cells were transfected with plasmids expressing either human c-Jun (encoded by the gene *JUN*) or SOX2 and co-expressing eGFP under a CMV promoter, and cells expressing eGFP under the same promoter were used as a control. Compared to control HEK cells, in which c-Jun or SOX2 proteins were not detected by immunofluorescence (IF), transfection of c-Jun- or SOX2-containing plasmids led to strong expression of each protein in eGFP-positive cells (Fig. 4A) and at the mRNA level (Fig. 4B). We then obtained exosomes from control HEK cells and from HEK cells overexpressing SOX2 or c-Jun, and treated DRG sensory neurons with the purified exosomes. As expected, control HEK cell exosomes had no effect on neurite growth compared to the effect of vehicle treatment (Fig. 4C,D). Impressively, exosomes from HEK cells overexpressing either c-Jun or SOX2 strongly stimulated neurite growth (Fig. 4C,D). Importantly, these effects on neurite extension were not due to differences in exosome internalization by sensory neurons (Fig. S3A,B). These results suggest that transcriptional programs controlled by c-Jun and SOX2 are involved in the capacity of exosomes to promote neurite extension, an effect that is likely associated with modulation of the exosomal cargo.

The miRNA cargo of rSC exosomes is involved in their pro-growth effect on neurites

Exosomes are highly enriched in miRNA molecules, which appear to be determinants of several biological roles of exosomes. Therefore, we studied whether the effect of rSC exosomes on neurite extension was associated with miRNA cargoes. We first used ultraviolet (UV) treatment as a non-specific method to damage the RNA molecules contained in rSC exosomes (Eldh et al., 2010; Zhang et al., 2016). Indeed, rSC exosomes treated with UV lost their

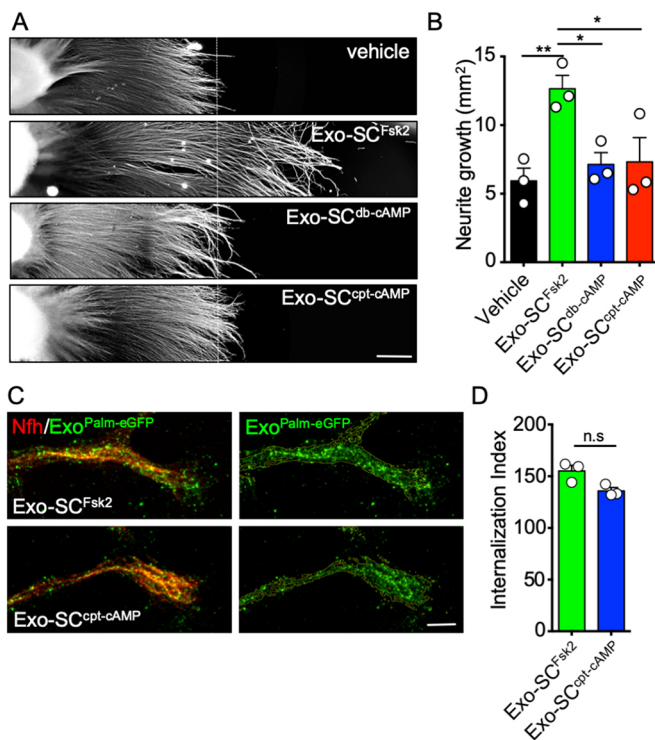


Fig. 2. Exosomes derived from rSCs, but not from dSCs, enhance neurite growth. (A) Neurite growth from DRG explants. SC exosomes from each condition (Fsk2 or cAMP analogs) were administered daily for 3 d at a final concentration of 120 ng/ml. After 3 d, DRG were visualized using immunostaining against acetylated tubulin. Dashed line indicates the neurite growth front of the vehicle control condition. Scale bar: 250 μ m. (B) Neurite growth area was quantified by measuring the neurite growth area minus explant body area. Mean \pm s.e.m. neurite growth of DRG neurons is shown. $n=3$. * $P<0.05$, ** $P<0.001$ (ANOVA followed by Bonferroni post-test). (C) Exosomes from Fsk2- and cAMP-treated SCs were isolated from palm-eGFP-transduced cells. DRG explants were treated with 5 μ g of eGFP-labeled exosomes for 3 h, washed and immunostained to detect neurofilament heavy chain (NfH, red) and eGFP (green). Scale bar: 2 μ m. (D) The internalization index was obtained from confocal images and deconvolved z-stack images by measuring the mean eGFP staining area that colocalized with NfH staining. Mean \pm s.e.m. internalization index was calculated from five neurites from three separate experiments. n.s., not significant (two-tailed *t*-test).

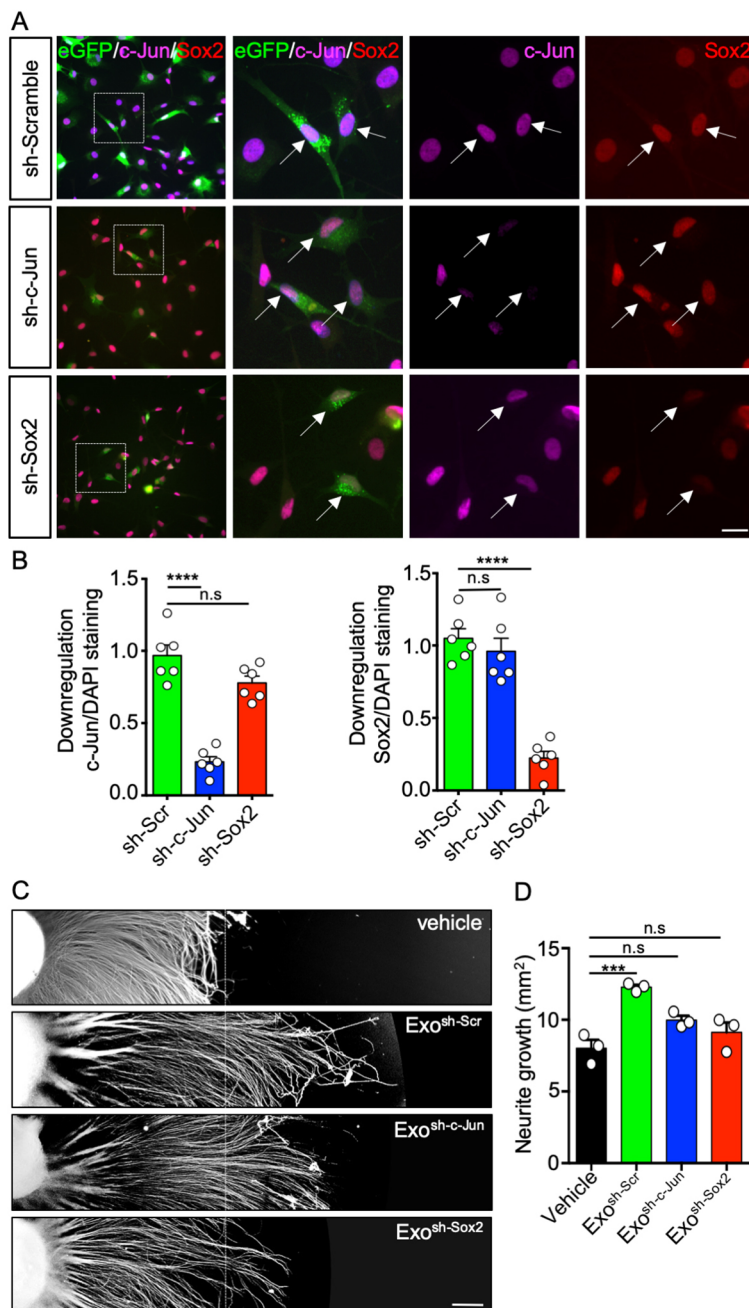


Fig. 3. Sox2 and c-Jun expression modulates the growth capacity of rSC exosomes. SCs cultured under 2 μ M forskolin (Fsk2) were transduced with shRNA against c-Jun or Sox2, which also expressed eGFP to allow identification of transduced cells. Exosomes from these cells were isolated. A scrambled shRNA expressing eGFP was used as control (sh-Scramble). (A) Immunostaining against c-Jun (magenta) or Sox2 (red) in shRNA transduced SCs. DAPI was used to stain nuclei (blue). Arrows show eGFP-positive SCs in each condition. Boxes in left panels indicate regions shown as magnifications in the panels on the right. Scale bar: 25 μ m. (B) Quantification of shRNA effect on protein expression by measuring staining density of Sox2 or c-Jun in shRNA-transduced SCs. A total of 15 cells were analyzed from each experiment and the mean \pm s.e.m. of six separate experiments is shown. **** P < 0.00001; n.s., not significant (ANOVA followed by Bonferroni post-test). (C) Neurite growth from DRG explants treated for 3 d with 120 ng/ml of exosomes from rSCs transduced with sh-scramble (sh-Scr), sh-Sox2 or sh-c-Jun. A DRG explant treated for 3 d with vehicle solution is included for comparison. DRG were immunostained against acetylated tubulin. Dashed line indicates the neurite growth front of the vehicle control condition. Scale bar: 250 μ m. (D) Neurite growth was quantified by measuring the neurite growth area minus explant body area. Mean \pm s.e.m. neurite growth of DRG neurons is shown. n = 3. *** P < 0.0005; n.s., not significant (ANOVA followed by Bonferroni post-test).

capacity to enhance neurite growth (Fig. 5A,B). We then used a genetic approach to establish whether miRNAs contained in rSC exosomes are required for neurite extension. To this end, an shRNA against *Dicer1*, which encodes a key protein in miRNA maturation (Lee et al., 2002), was virally expressed in rSCs, and exosomes from these cultures were tested for their capacity to enhance neurite growth. Compared to exosomes derived from rSCs transduced with a scrambled shRNA, neurite extension was significantly reduced when neurons were treated with exosomes derived from rSCs expressing *Dicer1* shRNAs (Fig. 5C,D). Having established the possible participation of rSC exosome miRNAs in promotion of neurite extension, we determined the miRNA expression profile of rSC exosomes and rSCs by next-generation small RNA sequencing. Sequences were aligned to known miRNA sequences obtained from miRbase. The correlation plot and principal component analysis

(PCA) of our RNAseq expression data demonstrated that miRNAs from rSC and exosome samples segregated, but were highly similar within each group (Fig. S4A,B). Absolute quantification of miRNAs demonstrated that only a small pool of rSC miRNAs are contained in exosomes, with some exosomal miRNAs found at similar proportions in rSCs, whereas other miRNAs were found to be overrepresented in rSC-derived exosomes (Fig. 5E; Fig. S4C). We next analyzed miRNAs with high raw RNAseq read counts in rSC exosome samples (Fig. 5E,F). Interestingly, several of them have been shown to modulate different neuronal processes, including axonal growth and regeneration (data not shown). Especially interesting was the high expression of miRNA-21 in exosomes from rSCs, as this miRNA has been implicated in cell-autonomous enhancement of axonal growth *in vitro* (Strickland et al., 2011).

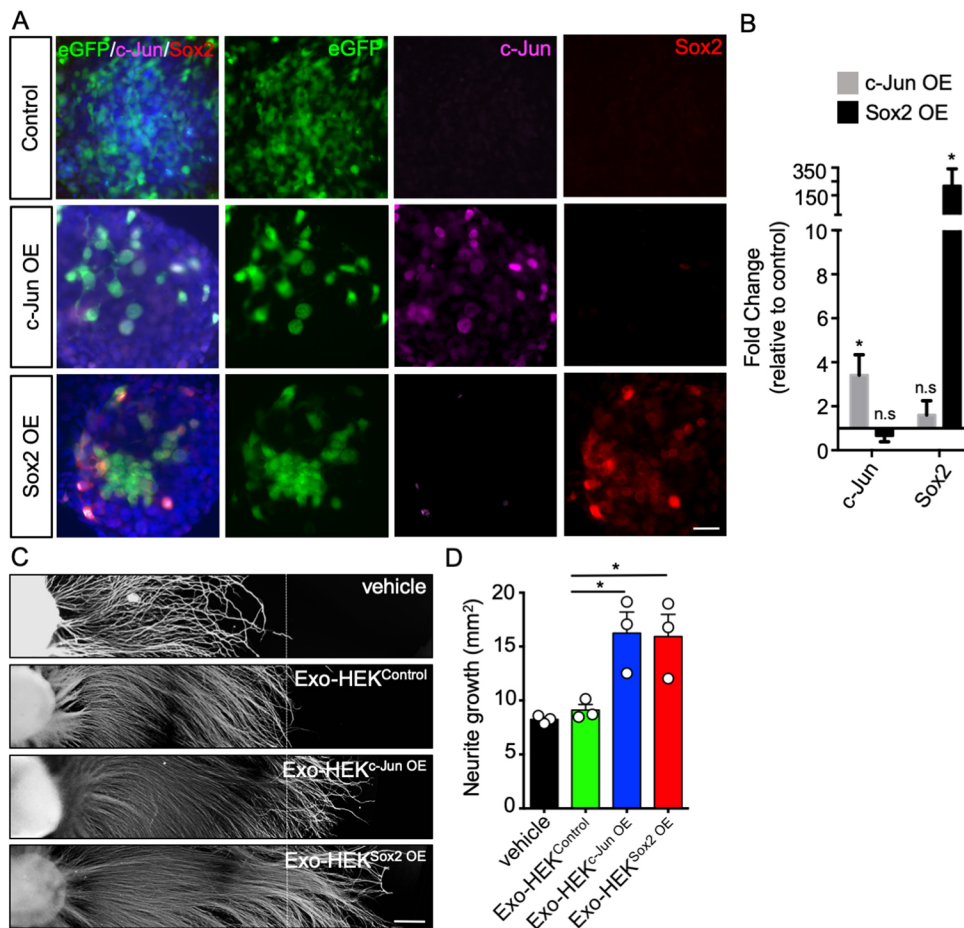


Fig. 4. Overexpression of human c-Jun or SOX2 produces regenerative HEK exosomes. (A) HEK 293T cells were transfected with plasmids to overexpress human c-Jun or SOX2 together with eGFP. An empty eGFP vector was used as a control. Cells were immunostained for c-Jun (magenta) and SOX2 (red), together with eGFP (green) and DAPI (blue). (B) RT-qPCR analysis of *JUN* (c-Jun) and *SOX2* mRNAs in HEK cells transfected with c-Jun (gray bars) or SOX2 (black bars) plasmids, relative to eGFP-transfected cells. Data are mean±s.e.m. of triplicate experiments. n.s., non-significant; * $P<0.05$ (ANOVA followed by Bonferroni post-test). (C) Neurite growth from DRG explants treated for 3 d with 120 ng/ml of exosomes isolated from conditioned medium of HEK cells transfected with a control vector (Exo-HEK^{Control}), c-Jun (Exo-HEK^{c-Jun OE}) or SOX2 (Exo-HEK^{Sox2 OE}). DRG were visualized using acetylated tubulin immunostaining. Dashed line indicates the neurite growth front of the vehicle control condition. Scale bar: 250 μ m. (D) Neurite growth was quantified by measuring the neurite growth area minus explant body area. Mean±s.e.m. neurite growth of DRG neurons is shown. $n=3$. * $P<0.05$ (ANOVA followed by Bonferroni post-test).

SC reprogramming upregulates exosomal miRNA-21 to promote neurite growth

Our data suggest that miRNAs contained in rSC exosomes mediate their pro-regenerative capacity. Furthermore, profiling of the miRNAs of rSC exosomes demonstrated the enrichment of several miRNAs with reported neuronal-autonomous effects on axonal regeneration and neurite growth. We focused on miRNA-21, due to its known effects on neurite growth (Strickland et al., 2011). Interestingly, relative to dSCs (cpt-cAMP-treated), rSCs (Fsk2-treated) have increased expression of miRNA-21 (Fig. 6A), and miRNA-21 expression was also strongly increased in exosomes derived from rSCs compared to those obtained from dSCs (Fig. 6B). We then functionally tested whether miRNA-21 was involved in the enhancement of neurite extension exhibited by rSC exosomes. To this end, rSCs were transfected with an miRNA-21 inhibitor, and exosomes from these SCs were used for growth assays. Compared to treatment with exosomes derived from rSCs transfected with a non-targeting oligonucleotide, neurite extension was significantly reduced when neurons were treated with exosomes derived from rSCs expressing the miRNA-21 inhibitor (Fig. 6C,D). Using a similar approach, we also tested two other miRNAs that were highly abundant in rSC exosomes, miRNA-10b and miRNA-27b. We found that inhibition of these miRNAs had no effect on neurite extension (Fig. 6C,D), suggesting some specificity of miRNA-21 in the exosome-derived enhancement of neurite extension. One of the known targets of miRNA-21 is PTEN (phosphatase and tensin homolog), which is a well-known negative regulator of neurite growth through its inhibitory effect on PI3K–Akt signaling (Duraikannu et al., 2019; Ohtake et al., 2015). Therefore, we

studied whether miRNA-21-loaded exosomes modulated PTEN levels in receiving neurons. Indeed, treatment with rSC-derived exosomes led to a significant downregulation of *Pten* mRNA in DRG neurons (Fig. 6E). Having established that PTEN expression is modulated after exosome treatment, we then studied the involvement of PI3K in the pro-growth effect of rSC exosomes. To this end, we pharmacologically inhibited PI3K using wortmannin. Compared to vehicle-treated DRGs, wortmannin treatment alone had no effect on neurite growth; nevertheless, it completely suppressed the pro-growth effect of rSC-derived exosomes (Fig. 6F,G). This suggests that rSC exosomes activate a signaling pathway for enhancement of neurite growth that is different to the one driving neurite growth under basal conditions. Taken together, this data demonstrates that reprogramming of SCs to the rSC phenotype enhances expression of miRNA-21, which has a pro-regenerative effect on sensory neurons by modulating the PI3K signaling pathway.

DISCUSSION

The role of SCs in promoting axonal regeneration in the peripheral nervous system (PNS) has been widely documented (Zochodne, 2012). The pro-regenerative capacity of rSCs has been attributed to their ability to perform several processes in the injured nerve, including secretion of pro-regenerative and pro-survival molecules, the formation of cellular tracks for axonal growth and mounting an innate immune response (Jessen and Mirsky, 2019). Here, we demonstrate that the reprogramming of SCs to a repair phenotype is accompanied by the secretion of regenerative exosomes, characterized by a repair-specific miRNA cargo that enhances

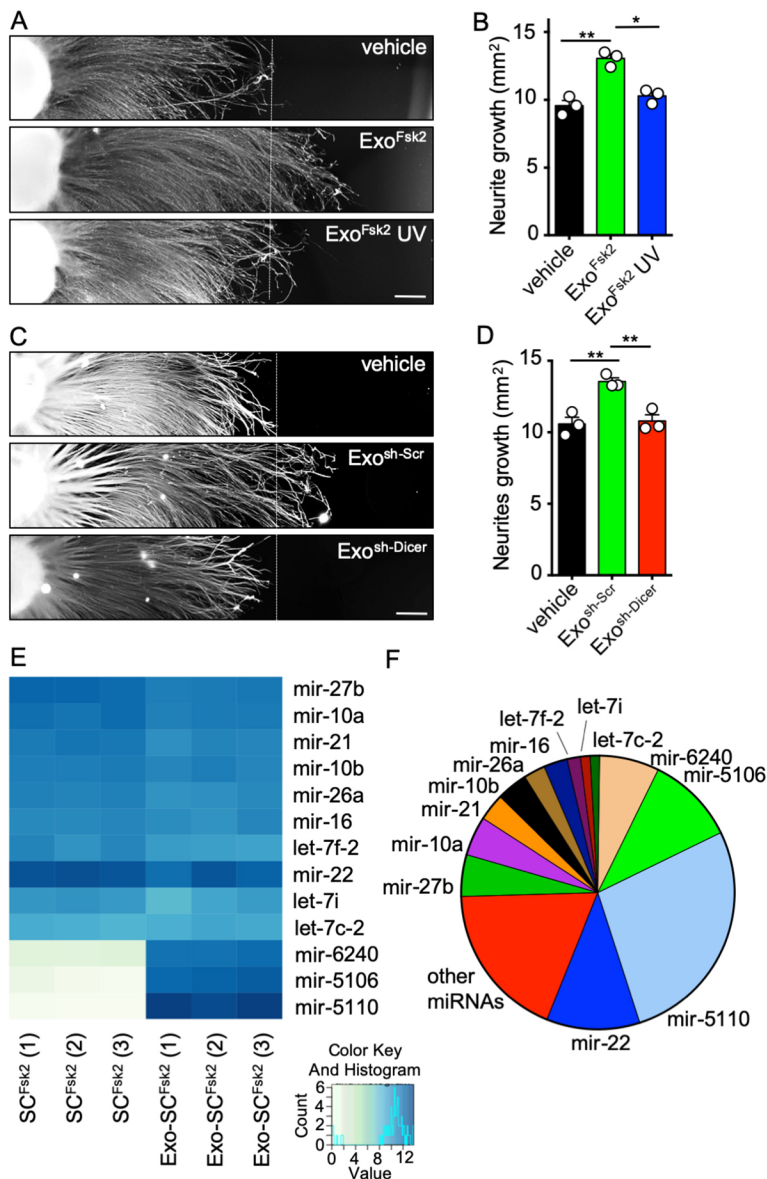


Fig. 5. The miRNA cargo of rSC exosomes is involved in their pro-growth effect on neurites. (A) Exosomes from rSCs were UV irradiated for 1 h on ice and used to treat DRG daily for 3 d at a concentration of 120 ng/ml, and the effects compared to treatment with non-irradiated control rSC exosomes or vehicle. DRG were visualized using acetylated tubulin immunostaining. Dashed line indicates the neurite growth front of the vehicle control condition. Scale bar: 250 μ m. (B) Neurite growth was quantified by measuring the neurite growth area minus explant body area. Mean \pm s.e.m. neurite growth of DRG neurons is shown. $n=3$. * $P<0.05$, ** $P<0.001$ (ANOVA followed by Bonferroni post-test). (C) Downregulation of Dicer in rSCs by transduction with a lentivirus coding for sh-RNA against Dicer. sh-RNA against a scrambled sequence was used as a control. Exosomes isolated from each condition were administered to DRG daily for 3 d at a final concentration of 120 ng/ml. DRG were visualized using acetylated tubulin immunostaining. Dashed line indicates the neurite growth front of the vehicle control condition. Scale bar: 250 μ m. (D) Neurite growth was quantified by measuring the neurite growth area minus explant body area. Mean \pm s.e.m. neurite growth of DRG neurons is shown. $n=3$. ** $P<0.001$ (ANOVA followed by Bonferroni post-test). (E) Small RNAseq analysis of cellular and exosome-derived miRNAs from rSCs. Heat map showing normalized expression levels (in triplicate) of the 13 miRNAs with highest expression in rSC exosomes (Exo-SC^{Fsk2}) and compared to the expression in rSCs (SC^{Fsk2}). Blue corresponds to highest expression and white to lowest expression. Columns represent data sets and rows represent miRNAs. (F) Pie chart showing the percentage expression of the 13 miRNAs with highest expression in rSC exosomes relative to the total identified exosomal miRNA.

neurite growth. To our knowledge, this is the first report to show that SC reprogramming leads to a modification of the miRNA cargoes of their secreted exosomes, adding a novel dimension to the reprogramming event – the differential properties of exosomes. It will be important to assess whether rSC exosomes are also involved in critical features of rSCs associated with the degenerative and regenerative response after nerve damage, including neuronal survival, cell adhesion and immune responses. In fact, we found that rSC exosomes contained miRNAs that are reported to be involved in diverse functions, including cellular adhesion and modulation of immune activities. Furthermore, a recent proteomic analysis of rSC exosomes showed that they contain proteins associated with different biological processes, including cell adhesion, angiogenesis and immune responses (Wei et al., 2019).

Although the model we used to produce dSCs *in vitro* mimics several characteristics of dSCs *in vivo*, it is important to consider that axonal contact is missing, which is known to influence the SC phenotype. Nevertheless, our *in vitro* system is suitable to analyse, by different ‘omics’ techniques, the changes in the SC secretome associated with reprogramming of SCs, including changes in

protein and RNA content. Having established that certain miRNAs are modulated after SC reprogramming *in vitro*, it will be important to corroborate these findings in an *in vivo* setting. Identification of miRNAs highly expressed in exosomes, but with low expression in the secreting rSCs (Fig. 5E), will allow the generation of tagged molecules to study this process during *in vivo* regeneration after peripheral nerve damage.

The loss-of-function experiments downregulating c-Jun or Sox2 in rSCs might shift the SC phenotype into a differentiated state (dSC) and therefore modulate the content of their derived exosomes, decreasing their neurite growth properties. Although this remains a possibility, our gain-of-function experiments upregulating c-Jun and SOX2 transcription factors in HEK cells demonstrated that the neurite growth capacity of cellular exosomes can be directly controlled by targets of these transcription factors, independent of the differentiation state of the cell. Indeed, transcription factors regulate miRNA expression at the transcriptional level (Treiber et al., 2019; Wang et al., 2010). Importantly, in conditions with poor regenerative outcomes, including advanced age and chronic denervation, rSCs have decreased levels of c-Jun expression,

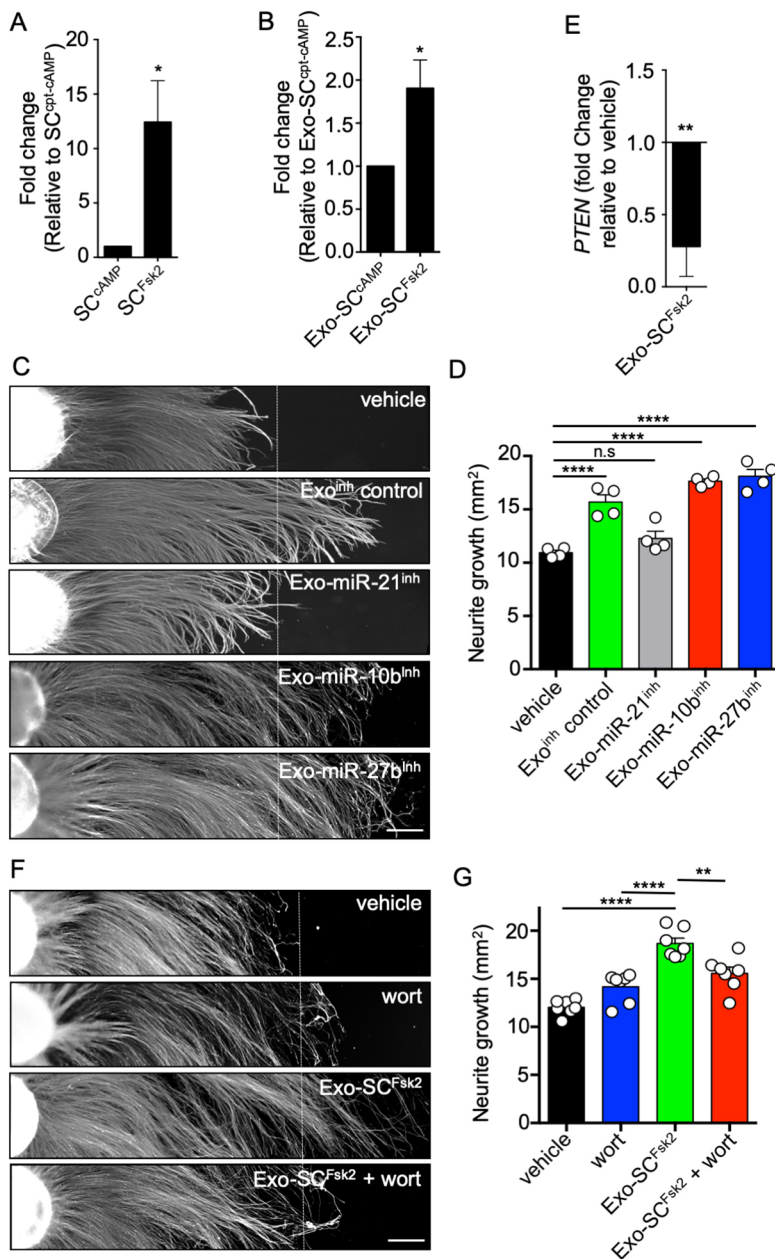


Fig. 6. SC reprogramming upregulates exosomal miRNA-21, promoting neurite growth. (A,B) RT-qPCR of miRNA-21 from SCs treated with Fsk2 and cAMP and from exosomes derived from the SC cultures. (C) *elegans* cel-miR-39 was spiked into each sample and used to normalize the levels of RNA input. The quantification of PCR products was performed using the $2^{-\Delta\Delta C_t}$ method. Data are mean \pm s.e.m. of assays performed in triplicate. * $P < 0.05$ (ANOVA followed by Bonferroni post-test). (D) Neurite growth from DRG explants. Oligonucleotide inhibitors for miR-21, miR-10b and miR-27b, and a non-targeting inhibitor (control), were transfected into rSCs and exosomes from these preparations were isolated. Exosomes isolated from each condition were administered to DRG daily for 3 d at a final concentration of 120 ng/ml. DRG were visualized using acetylated tubulin immunostaining. Dashed line indicates the neurite growth front of the vehicle control condition. Scale bar: 250 μ m. (E) Neurite growth was quantified by measuring the neurite growth area minus explant body area. Mean \pm s.e.m. neurite growth of DRG neurons is shown. $n = 4$. **** $P < 0.0001$; n.s., not significant (ANOVA followed by Bonferroni post-test). (F) RT-qPCR of DRG treated with rSC exosomes was performed to analyze the levels of *Pten* mRNA compared to levels in vehicle-treated DRG neurons. Data were normalized to *Gapdh* expression. The quantification of PCR products was performed using the $2^{-\Delta\Delta C_t}$ method. Data are mean \pm s.e.m. of assays performed in triplicate. ** $P < 0.001$ (ANOVA followed by Bonferroni post-test). (G) DRGs were treated daily with vehicle, Exo-SC^{Fsk2} at 120 ng/ml and/or 100 nM of wortmannin (wort) for 3 d. DRG were visualized using acetylated tubulin immunostaining. Dashed line indicates the neurite growth front of the vehicle control condition. Scale bar: 250 μ m. (H) Neurite growth area was quantified by measuring the neurite growth area minus explant body area. Mean \pm s.e.m. neurite growth of DRG neurons is shown. $n = 7$. ** $P < 0.001$, **** $P < 0.0001$ (ANOVA followed by Bonferroni post-test).

which has been functionally associated with a decrease in the pro-regenerative capacity of SCs (Painter et al., 2014). Whether diminished levels of c-Jun in rSCs after nerve damage in aged organisms or after chronic denervation leads to a modification to the miRNA content of exosomes, thereby affecting axonal regeneration, remains to be established.

Our studies on the miRNA profile of rSCs and their derived exosomes suggested that some miRNAs are specifically cargo, and are secreted in SC exosomes. Asymmetric miRNA and mRNA distributions between cells and their exosomes have been previously reported in other cell types (Ragusa et al., 2017). Different sorting mechanisms for asymmetric miRNA expression in exosomes has been described, including those controlled by specific miRNA motifs (Santangelo et al., 2016; Villarroya-Beltri et al., 2013), as well as regulation by cellular levels of the target transcripts (Squadrito et al., 2014). Our bioinformatic analysis failed to identify specific target sequences in miRNAs asymmetrically overexpressed

in rSC exosomes (data not shown). We focused on miRNA-21, because this RNA has been associated with the regulation of axonal guidance and was highly expressed in rSC exosomes. Interestingly, miRNA-21 has been shown to be a direct target of c-Jun in vascular endothelial cells (Zhou et al., 2011), and the AP-1 early response transcription factor, composed of c-Jun and c-Fos, positively regulates the expression of miRNA-21 in cancer cell lines (Fujita et al., 2008). In the PNS, the miRNA-21 passenger strand miRNA-21-3p is expressed at much lower levels in c-Jun-null injured nerves than in control injured nerves (Arthur-Farraj et al., 2017). Our data demonstrated that miRNA-21 is required for the effects of rSC exosomes in neurite extension, which could be due to the downregulation of diverse mRNA targets of miRNA-21, including *PTEN*, *Sprouty2* (*Spry2*) and *Ephrin*, all reported to contribute negatively to neurite extension. *PTEN* deletion or knockdown greatly enhances axonal regeneration in the PNS (Christie et al., 2010), as well as axonal regeneration in the optic

nerve and corticospinal neurons (Park et al., 2008; Liu et al., 2010; Zukor et al., 2013; Geoffroy et al., 2015). Related to PTEN downregulation by rSC-derived exosomes, our experiments demonstrated that the enhancement of neurite growth by rSC exosomes is dependent on the activation of PI3K, which has well-known roles in axonal growth and regeneration after injury (Ohtake et al., 2015). Nevertheless, inhibition of PI3K in untreated DRGs had no effect on neurite growth, suggesting that at least two pathways for neurite extension operate in sensory neurons, a basal one that is dependent on the NGF added to the culture medium, which probably activates extracellular signal-related kinases (ERK) or phospholipase C- γ (Denk et al., 2017), and a PI3K-dependent pathway activated by rSC exosomes. Additionally, it is important to consider that paracrine factors secreted by rSCs have well-known pro-regenerative roles *in vitro* and *in vivo* (Schira et al., 2019; Johnston et al., 2016). In our *in vitro* model, neurite growth is critically dependent on supplemented NGF (Kaselis et al., 2014), which emulates the factors secreted by rSCs and other cells present in the developing and regenerating nerve. This might explain why rSC-conditioned medium did not further enhance neurite growth (Fig. S2A,B) in an NGF-saturated culture condition.

The role of miRNA in SC development and myelination has been studied using conditional knockdown of Dicer in SCs. Dicer expression is required for SC differentiation and proper developmental myelination (Verrier et al., 2010). Interestingly, Dicer deletion in adult SCs causes progressive axonal degeneration (Li et al., 2018), and using an injury paradigm together with similar approaches for time- and cell-specific deletion of Dicer, leads to a delay in the transition from dSC to rSC in peripheral nerves (Viader et al., 2011). Although regeneration was not affected, this process was only studied at later time points following nerve crush (14 d post-damage) and at a single nerve level (Viader et al., 2011). Therefore, more detailed studies on nerve regeneration will be required to establish the role of exosomal miRNA in nerve regeneration. We have found that rSC exosomes lead to a profound change in the transcriptomic profile of receiving sensory neurons (data not shown), therefore the effect of exosomes on neurite growth probably involves modulation of several mRNAs, as well as direct mRNA and protein transfer by exosomes and activation of signaling cascades in sensory neurons. More studies will be required to dissect the diverse effects of exosomes on neurons, which probably modulate diverse neuronal programs depending on the cellular context.

Our work suggests that the transfer of exosomes from SCs to neurons is part of the repair program mounted by SCs after nerve injury, probably contributing to axonal regeneration and functional recovery after nerve injury. This not only underscores a cellular mechanism for non-cell-autonomous regulation of neuronal function but also provides novel strategies to enhance axonal regeneration in poor regenerative regions of the nervous system or in conditions where regeneration is greatly impaired, including aging and chronic denervation.

MATERIALS AND METHODS

Schwann cell culture

SCs were obtained from newborn P2–P3 SD rat sciatic nerves as previously described (Lopez-Verrilli et al., 2013; De Gregorio et al., 2018), expanded over laminin coating and maintained on DMEM with 10% FBS (Gibco Life Technologies, cat. #10437028) supplemented with 2 μ M forskolin (Sigma, cat. #F3917) and 20 μ g/ml bovine pituitary extract (BPE; Gibco Life Technologies, cat. #1302814). The medium was replaced every 3 d until the cells reached 90% confluency. All experiments with SCs were performed with cells at early passage of P3–P4. Animal procedures were carried out in

accordance to the Institution's Animal Care Committee Guidelines. For pharmacologic induction experiments, cells were seeded at 50,000 cells/cm² in T175 flasks for exosome isolation or in 24-well plates for IF. Cells were cultured for 48 h and then changed to the induction medium (DMEM with 1% FBS, exosome-free). After 24 h, pharmacological agents were administered for 5 d at the following concentrations: db-cAMP, 1 mM (Sigma, cat. #D0260); cpt-cAMP, 250 μ M (Sigma, cat. #C3912); forskolin, 2 μ M (Sigma, cat. #F3917). After this time, conditioned medium was collected, and cells prepared for downstream analysis.

Rat embryonic dorsal root ganglia culture

DRG explants were prepared as previously described (López-Leal et al., 2018). Briefly, DRG were dissected from the spinal cord of E16.5 rat embryos. DRG were seeded in 96-well plates coated with poly-L-lysine/collagen type I and neurobasal medium supplemented with 1 \times B27 (50 \times , Gibco), 20 μ M L-glutamine, 1 \times antibiotic-antimycotic solution (100 \times , Gibco), 3.75 μ M aphidicolin (Sigma, cat. #A0781), 1.25 μ M 5-fluoro-2-deoxyuridine (Sigma, cat. #F0503) and 50 ng/ml of nerve growth factor (NGF-2.5s; Thermo Fisher Scientific, cat. #13257-019). Isolated exosomes were administered daily at a final concentration of 120 ng/ml. Wortmannin (Calbiochem cat. # 195545-26-7) was added daily at 100 nM for 3 d. After 3 d in culture, DRG were fixed in 4% paraformaldehyde (PFA). IF against acetylated tubulin was performed as described below, photo-documented using an automated Leica DMI8 microscope together with Las-X software, and neurite growth area was quantified using ImageJ (NIH, MD). All animal procedures were carried out in accordance with the Institutional Animal Care Committee guidelines.

HEK 293T culture and transfection

HEK 293T cells were maintained on 100 mm plates on DMEM with 10% FBS. The culture medium was changed every 3 d. For exosome isolation, HEK cells were grown in a 150 mm plate in DMEM, 4% FBS exosome-free. For overexpression experiments, HEK 293T cells were seeded at 12 \times 10⁶ cells on a 150 mm plate for 24 h before transfection. The CaCl₂ method was used to transfect 40 μ g of target vector (Graham and van der Eb, 1973). Vectors used in this study were produced by Vigene Bioscience, USA: pLenti-CMV-SOX2-P2A-GFP (NM_003106.3); pLenti-CMV-JUN-P2A-GFP (NM_002228). An empty vector, pLenti-CMV-Empty-P2A-GFP, was used as control.

Exosome isolation

Exosomes were isolated by differential ultracentrifugation using a micro-ultracentrifuge CS ISONX Himac Hitachi equipped with a S58A rotor as described (De Gregorio et al., 2018). In brief, pooled conditioned medium (CM) was collected from SCs incubated with induction culture medium supplemented with 1% exosome-depleted FBS. To discard cellular debris and dead cells, CM was centrifuged at 2000 *g* for 10 min at room temperature. Then, to discard microvesicles, the supernatant was centrifuged at 11,000 *g* for 30 min at 4°C. To pellet exosomes the supernatant from the last step was centrifuged at 100,000 *g* for 1 h at 4°C. The exosome pellet was washed with 5 ml of filtered PBS and centrifuged again at 100,000 *g* for 1 h at 4°C. Finally, the exosome pellet was resuspended in 100 μ l of filtered PBS and stored at –20°C until use. Exosomes were quantified by analyzing the protein content of purified exosomes. To this end, a modified BCA protein assay (Pierce cat. # 23225) for higher sensitivity was performed for all exosome samples. Table S1 shows detail of protein concentration per volume of conditioned medium collected, and the corresponding number of exosomes detected using a Nanosight (Malvern NS300).

Isolation of rSC exosomes and rSC-conditioned medium without exosomes

For the purification of exosomes, 30 ml of conditioned medium was used. Exosomes were isolated by differential ultracentrifugation as described above. The supernatant from the last step was centrifuged at 100,000 *g* for 1 h at 4°C and then the medium without exosomes was collected. The exosome pellet was washed with 5 ml of filtered PBS and centrifuged again at 100,000 *g* for 1 h at 4°C. Finally, the exosome pellet was resuspended in

100 µl of filtered PBS and stored at −20°C until use. DRG explants were prepared as described above. Isolated exosomes were administered daily at a final concentration of 120 ng/ml and the SC-conditioned medium without exosomes was prepared by mixing 60% of 100,000 *g* supernatant fraction with 40% of complete neurobasal medium for DRG incubation. The mixed medium was replaced daily for 3 d.

Lentivirus generation

HEK 293T cells were grown at 37°C with 5% CO₂ in a humidified incubator. The culture medium contained DMEM supplemented with 10% FBS, and penicillin-streptomycin (50 U/ml and 50 µg/ml, respectively). For lentivirus preparation, HEK 293T cells were seeded at a density of 12×10⁶ cells on a 150 mm plate 24 h before transfection. Lentivirus was produced by transfecting HEK 293T cells with the lentiviral vector Palm-eGFP (Xandra Breakefield, Massachusetts General Hospital, Charlestown, MA) and two helper plasmids (pVSVg, delta8.9; Addgene, plasmid numbers 12263, 12259 and 8454), by the calcium phosphate precipitation method (Zufferey et al., 1997). Plasmids were mixed as follows: 20 µg of the Palm-eGFP vector, 10 µg of pVSVg and 15 µg of delta 8.9. To this mix, 400 µl of 1.25 M CaCl₂ plus 1.5 ml H₂O were added. This solution was added dropwise to the cells. After 4 h, the medium was changed with fresh growth medium. After 2 d, the conditioned medium was harvested and centrifuged at 2000 *g* for 7 min. The supernatant was then filtered using a 0.45 µm filter. This preparation was then concentrated using the Lenti-X concentrator (Takara) following the manufacturer's instructions.

Lentiviral transduction of SCs

SCs at 40% confluency were treated with 5 µg/ml polybrene (Sigma, cat. #H9268). Then, lentivirus particles were added to the plate at 1×10⁶ transduction units/ml for 24 h. After that, the medium was changed for fresh growth medium. Lentiviruses encoding four shRNAs were used to downregulate Sox2 and c-Jun (pLenti-4in1-GFP-JUN, pLenti-4in1-GFP-SOX2; Vigene Biosciences). Scrambled shRNA sequence was used as control (pLenti-U6-GFP-puro-scrambled shRNA; Vigene Biosciences). For Dicer downregulation, rat sh-dicer1-pLenti-3in1 shRNA-copGFP-P2A-puro (XM_001068155.3; Vigene Biosciences) was used to transduce SCs. The following sequences were used for shRNA studies. sh-Sox2: 5'-AG-CTACGCGACATGAACGGCTGGAGCAA-3', 5'-CAGTACAACCTCC-ATGACCAGCTCGACATC-3', 5'-GGCTCTGTGGTCAAGTCCGAG-GCCAGTTC-3', 5'-CCGTTTCATCGACGAGGCCAAGCGGCTGCG-3'. sh-c-Jun: 5'-CCGAGCCAAAGAACTCGGACCTTCTCACGT-3', 5'-TCT-GAAGCCGCACCTCCGAGCCAAAGAACT-3', 5'-TGAGGAACCGCA-TGCTGCTCCTCAAGTGC-3', 5'-AGCTGGCGTCCACGGCCAACA-TGCTCAGG-3'. sh-Dicer: 5'-GCTACACAGGAAGTTCTTA-3', 5'-GG-GAAAGTCTGCAGAACAA-3', 5'-CCTCATAACCAAGCACCTT-3'.

Internalization assay

SCs were transduced at 40–50% confluency with a lentivirus coding for CMV-Palm-eGFP (Lai et al., 2015). SC growth medium was replaced with induction medium 5 d after transduction. After 2 d, the induction medium was changed and replaced with fresh induction medium. Then, conditioned medium was collected from this cell culture after 3 d. Exosomes were isolated and quantified. A total of 5 µg of exosome proteins was incubated for 3 h with DRG previously grown for 3 d. Cells were imaged with a Leica confocal microscope TCS SP8. Las-X Leica software was used to deconvolve z-stack images, and internalization was assessed by measuring the eGFP staining area that colocalized with the NfH staining.

Immunofluorescence

IF analysis was performed as described previously (López-Leal et al., 2018). Briefly, culture medium was removed from wells containing SCs or DRG and washed 2–3 times with PBS. Then, the cells were fixed with 4% PFA for 15 min at room temperature. After washing, the cells were blocked and permeabilized with PBS containing 0.1% Triton X-100, 2% (v/v) fish skin gelatin (Sigma, cat. N°G7765) for 2 h at room temperature in a humidified chamber. Then, the cells were incubated with primary antibodies diluted in PBS containing 0.1% Triton X-100 and 1% (v/v) fish skin gelatin overnight at 4°C in a humidified chamber. The primary antibody was removed and cells

washed with PBS three times every 5 min at room temperature. Then, the cells were incubated with secondary antibodies diluted in washing solution for 2 h at room temperature in a dark humidified chamber. After removing the secondary antibodies, the cells were washed with PBS three times every 5 min at room temperature. Where nuclear staining was desired, the second PBS wash was replaced with DAPI staining. DAPI (stock concentration 5 mg/ml) was diluted 1:50,000 in PBS and incubated for 5 min at room temperature. Then, the cells were washed with PBS three times every 5 min at room temperature in a dark place. Finally, coverslips were mounted with mounting medium. Primary antibodies used were: rabbit anti-c-Jun, 1:200 (Cell Signaling Technology, cat. #9165); rabbit anti-Sox2, 1:500 (Cell Signaling Technology, cat. #2748); mouse anti-acetylated tubulin, 1:1000 (Sigma-Aldrich, cat. #T6793); rabbit anti-neurofilament heavy chain, 1:1000 (Sigma-Aldrich, cat. #N4142) and rabbit anti-myelin basic protein (MBP), 1:500 (Sigma-Aldrich, cat. #M3821). Secondary antibodies used were: anti-mouse Alexa Fluor-546 (Life Technologies, cat. #A11003); anti-rabbit Alexa Fluor-488 (Invitrogen, cat. #A11034); anti-goat Alexa Fluor-555, 1:1000 (Invitrogen, cat. #A27017) and anti-rabbit Alexa Fluor-647, 1:1000 (Invitrogen, cat. #A21244). Cells were imaged using a Leica microscope DMi8 equipped with a motorized stage. Objectives used were a Leica HC PL 10×/0.32 and a Leica 20×/0.40 HCX PL. Images were captured with Leica LAS X software version 2.0.

Reverse transcription quantitative PCR

For reverse transcription quantitative PCR (RT-qPCR) analysis, total RNA and microRNA isolation was performed using the RNeasy and miReasy miniprep kit (Qiagen). DNase treatment was performed on the column according to the manufacturer's protocol (Qiagen). cDNA was synthesized using iScript one-step reverse transcription, according to the manufacturer's instructions (Bio-rad). RT-qPCR was performed in the StepOnePlus (96-well) Real-Time PCR System using 5× HOT FIREPol EvaGreen qPCR Mix Plus and following the manufacturer's instructions. The sequences of the primers used to detect rat (*r*) *Sox2*, *Bdnf*, *Artn*, *Lif*, *Mbp* and *Gapdh* (internal control), as well as human (*Hs*) *JUN* (which encodes c-Jun) and *SOX2* are as follows: *rSox2* F, 5'-CAGCATGTCCTACTCGCAGCA-3'; *rSox2* R, 5'-GGAAGTGGCCTCGGACTTGA-3'; *rBdnf* F, 5'-AGCTGAGCGTGTG-TGACAGT-3'; *rBdnf* R, 5'-ACCATGGGATTACACTTGG-3'; *Gadph* F, 5'-TCCCTCAAGATTGTCAGCAA-3'; *Gadph* R, 5'-AGATCCACAAC-GGATACATT-3'; *rArtn* F, 5'-ATGTCGCCCTACCTGGAAC-3'; *rArtn* R, 5'-GGCTCT-GTCTGTCCCTCATC-3'; *rLif* F, 5'-TCAAACCTCAATGCG-ACTACAGA-3'; *rLif* R, 5'-ACACAGGGCACATCCACA-3'; *rMbp* F, 5'-CACAAGAAGTACCCACTACGG-3'; *rMbp* R, 5'-GCCTCTCCCCTTT-CCTTG-3'. *HsSox2* F, 5'-TACAGCATGTCCTACTCGCAG-3'. *HsSox2*, R 5'-GA-GGAAGAGGTAACCACAGG-3'. *HsJun* F, 5'-TCCAAGTGCC-GAAAAGGAAG-3'. *HsJun* R, 5'-CGAGTTCTGAGCTTTCAAGGT-3'.

The quantification of PCR products was performed using the 2^{−ΔΔC_T} method, and the quantity of mRNA was normalized to the housekeeping gene *Gapdh*. The assays were performed in triplicate. For quantitative miRNA analysis, microRNA cDNA was synthesized using MystiCq microRNA cDNA Synthesis Mix Kit and MystiCq MicroRNA quantification system (Invitrogen) using 20 ng of total RNA. Cel-miR39 was used as spike-in to normalize cDNA levels in exosome microRNA analysis.

miRNA inhibitions in SCs

For miRNA loss-of-function studies, LNA-enhanced antisense miRNA inhibitors labeled with FAM were used (Qiagen), and transfected into rSCs using Lipofectamine 2000 (ThermoFisher Scientific, cat. #11668027). The following sequences were used: miRNA-21 (MIR-21-5P), 5'-UAGCUU-AUCAGACUGAUGUUGA-3'; miRNA 27b (MIR-27b-3P), 5'-GCAGA-ACTTAGCCACTGTGA-3'; miRNA 10b (MIR-10b-5P), 5'-TAACACG-TCTATACGCCCA-3'; negative control A (YI00199006), 5'-TAACACG-TCTATACGCCCA-3'. For SC transfection and exosome isolation, the cells were grown to 70% confluency in a T75 flask. Then, 8 ml of Opti-MEM (Gibco, cat. #31985-070) was mixed with 10 nM of FAM-labeled oligonucleotide and 70 µl of Lipofectamine 2000. The mixed solution was incubated for 10 min at room temperature and then added to the cells. After 4 h in a cell incubator, the medium was replaced with growth medium. After 24 h,

the SC repair phenotype was induced using a low forskolin concentration (Fsk2) in the induction medium. After 72 h, exosomes were isolated and quantified as described above.

RNA-sequencing and data analysis

For SC and exosome RNA sequencing, SCs were grown in T175 flasks and 120 ml of conditioned medium was collected from four T175 flasks for each replicate then used for exosome isolation as described above. SC exosomes and SC cytoplasm total RNA was extracted using a miRNeasy Mini Kit from Qiagen. RNA quality was assessed using a 2100 Bioanalyzer (Agilent, USA) with a RNA 6000 Nano kit (Agilent Technologies, cat. #5067). Three independent replicates were further processed and sequenced. TruSeq Small RNA Libraries (Illumina) were prepared from 100 ng of total RNA, and RNA-sequencing was performed to generate 36 bp single-end reads on a HiSeq 2500 (Illumina). Reaper (Davis et al., 2013) was used to trim the 3' adapter sequence, and reads with length lower than 16 nucleotides and larger than 30 nucleotides were discarded using PRINSEQ (Schmieder and Edwards, 2011). Reads were aligned to *Mus musculus* and *Rattus norvegicus* hairpins from miRbase (Griffiths-Jones, 2005) (<ftp://mirbase.org/pub/mirbase/CURRENT/hairpin.fa.gz>) taking into account RNA folding predicted using RNAfold software from ViennaRNA Package 2.0 (Lorenz et al., 2011). Statistical analyses were conducted in R using the DESeq2 package from Bioconductor (Love et al., 2014). Spatial projection was analyzed by PCA using the *princomp* function in R. Hierarchical clustering and correlation plotting were performed on the normalized read count data as exploratory data analyses.

Statistical analysis

All data are presented as the mean \pm s.e.m. The comparison between groups was performed using a two-tailed Student's *t*-test. One-way ANOVA was used to evaluate the difference among multiple groups, followed by Bonferroni's multiple comparisons test. The data were analyzed using GraphPad Prism 6.0. *P*<0.05 was considered statistically significant.

Acknowledgements

We thank Xandra Breakefield (Massachusetts General Hospital, Charlestown, MA) for the palm-eGFP construct.

Competing interests

The authors declare no competing or financial interests.

Author contributions

Conceptualization: R.L.-L., F.A.C.; Methodology: R.L.-L., A.E., G.I.; Formal analysis: R.L.-L., F.D.-V., R.J.C., C.S., A.E., G.I.; Investigation: R.L.-L., F.D.-V., R.J.C., C.S.; Resources: F.A.C.; Writing - original draft: R.L.-L., F.A.C.; Writing - review & editing: R.L.-L., R.J.C., F.A.C.; Supervision: A.E., G.I., F.A.C.; Funding acquisition: F.A.C.

Funding

This work was supported by the Fondo Nacional de Desarrollo Científico y Tecnológico (FONDECYT-1150766), the Geroscience Center for Brain Health and Metabolism (FONDAP-15150012) and the Canada-Israel Health Research initiative (jointly funded by the Canadian Institutes of Health Research, the Israel Science Foundation, the International Development Research Centre, Canada and the Azrieli Foundation, Canada).

Data availability

Sequencing data generated in this work has been deposited at the NCBI repository under the BioProject accession PRJNA635900.

Supplementary information

Supplementary information available online at <http://jcs.biologists.org/lookup/doi/10.1242/jcs.239004.supplemental>

Peer review history

The peer review history is available online at <https://jcs.biologists.org/lookup/doi/10.1242/jcs.239004.reviewer-comments.pdf>

References

Arthur-Farraj, P. J., Latouche, M., Wilton, D. K., Quintes, S., Chabrol, E., Banerjee, A., Woodhoo, A., Jenkins, B., Rahman, M., Turmaine, M. et al.

- (2012). c-Jun reprograms schwann cells of injured nerves to generate a repair cell essential for regeneration. *Neuron* **75**, 633-647. doi:10.1016/j.neuron.2012.06.021
- Arthur-Farraj, P. J., Morgan, C. C., Adamowicz, M., Gomez-Sanchez, J. A., Fazal, S. V., Beucher, A., Razzaghi, B., Mirsky, R., Jessen, K. R. and Aitman, T. J. (2017). Changes in the coding and non-coding transcriptome and DNA methylome that define the schwann cell repair phenotype after nerve injury. *Cell Rep* **20**, 2719-2734. doi:10.1016/j.celrep.2017.08.064
- Boyd, J. G. and Gordon, T. (2003). Neurotrophic factors and their receptors in axonal regeneration and functional recovery after peripheral nerve injury. *Mol. Neurobiol.* **27**, 277-324. doi:10.1385/MN:27:3:277
- Chen, P., Piao, X. and Bonaldo, P. (2015). Role of macrophages in Wallerian degeneration and axonal regeneration after peripheral nerve injury. *Acta Neuropathol.* **130**, 605-618. doi:10.1007/s00401-015-1482-4
- Christie, K. J., Webber, C. A., Martinez, J. A., Singh, B. and Zochodne, D. W. (2010). PTEN inhibition to facilitate intrinsic regenerative outgrowth of adult peripheral axons. *J. Neurosci.* **30**, 9306-9315. doi:10.1523/JNEUROSCI.6271-09.2010
- Clements, M. P., Byrne, E., Camarillo Guerrero, L. F., Cattin, A.-L., Zakka, L., Ashraf, A., Burden, J. J., Khadayate, S., Lloyd, A. C., Marguerat, S. et al. (2017). The wound microenvironment reprograms schwann cells to invasive mesenchymal-like cells to drive peripheral nerve regeneration. *Neuron* **96**, 98-114.e7. doi:10.1016/j.neuron.2017.09.008
- Davis, M. P. A., van Dongen, S., Abreu-Goodger, C., Bartonicek, N. and Enright, A. J. (2013). Kraken: a set of tools for quality control and analysis of high-throughput sequence data. *Methods* **63**, 41-49. doi:10.1016/j.ymeth.2013.06.027
- De Gregorio, C., Diaz, P., López-Leal, R., Manque, P. and Court, F. A. (2018). Purification of exosomes from primary Schwann cells, RNA extraction, and next-generation sequencing of exosomal RNAs. *Methods Mol. Biol.* **1739**, 299-315. doi:10.1007/978-1-4939-7649-2_19
- Denk, F., Bennett, D. L. and McMahon, S. B. (2017). Nerve growth factor and pain mechanisms. *Ann. Rev. Neurosci.* **40**, 307-325. doi:10.1146/annurev-neuro-072116-031121
- Duraikannu, A., Krishnan, A., Chandrasekhar, A. and Zochodne, D. W. (2019). Beyond trophic factors: exploiting the intrinsic regenerative properties of adult neurons. *Front. Cell. Neurosci.* **13**, 128. doi:10.3389/fncel.2019.00128
- Eldh, M., Ekström, K., Valadi, H., Sjöstrand, M., Olsson, B., Jernäs, M. and Lötvall, J. (2010). Exosomes communicate protective messages during oxidative stress; possible role of exosomal shuttle RNA. *PLoS ONE* **5**, e15353. doi:10.1371/journal.pone.0015353
- Fazal, S. V., Gomez-Sanchez, J. A., Wagstaff, L. J., Musner, N., Otto, G., Janz, M., Mirsky, R. and Jessen, K. R. (2017). Graded elevation of c-jun in schwann cells *In Vivo*: gene dosage determines effects on development, remyelination, tumorigenesis, and hypomyelination. *J. Neurosci.* **37**, 12297-12313. doi:10.1523/JNEUROSCI.0986-17.2017
- Fujita, S., Ito, T., Mizutani, T., Minoguchi, S., Yamamichi, N., Sakurai, K. and Iba, H. (2008). miR-21 gene expression triggered by AP-1 is sustained through a double-negative feedback mechanism. *J. Mol. Biol.* **378**, 492-504. doi:10.1016/j.jmb.2008.03.015
- Gardiner, N. J. (2011). Integrins and the extracellular matrix: key mediators of development and regeneration of the sensory nervous system. *Dev. Neurobiol.* **71**, 1054-1072. doi:10.1002/dneu.20950
- Geoffroy, C. G., Lorenzana, A. O., Kwan, J. P., Lin, K., Ghassemi, O., Ma, A., Xu, N., Creger, D., Liu, K., He, Z. et al. (2015). Effects of PTEN and nogo codeletion on corticospinal axon sprouting and regeneration in mice. *J. Neurosci.* **35**, 6413-6428. doi:10.1523/JNEUROSCI.4013-14.2015
- Gomez-Sanchez, J. A., Carty, L., Iruarizaga-Lejarreta, M., Palomo-Irigoyen, M., Varela-Rey, M., Griffith, M., Hantke, J., Macias-Camara, N., Azkargorta, M., Aurrekoetxea, I. et al. (2015). Schwann cell autophagy, myelinophagy, initiates myelin clearance from injured nerves. *J. Cell Biol.* **210**, 153-168. doi:10.1083/jcb.201503019
- Graham, F. L. and van der Eb, A. J. (1973). A new technique for the assay of infectivity of human adenovirus 5 DNA. *Virology* **2**, 456-467. doi:10.1016/0042-6822(73)90341-3
- Griffiths-Jones, S. (2005). miRBase: microRNA sequences, targets and gene nomenclature. *Nucleic Acids Res.* **34**, D140-D144. doi:10.1093/nar/gkj112
- Hervera, A., De Virgiliis, F., Palmisano, I., Zhou, L., Tantardini, E., Kong, G., Hutson, T., Danzi, M. C., Perry, R. B.-T., Santos, C. X. C. et al. (2018). Reactive oxygen species regulate axonal regeneration through the release of exosomal NADPH oxidase 2 complexes into injured axons. *Nat. Cell Biol.* **20**, 307-319. doi:10.1038/s41556-018-0039-x
- Holm, M. M., Kaiser, J. and Schwab, M. E. (2018). Extracellular vesicles: multimodal envoys in neural maintenance and repair. *Trends Neurosci.* **41**, 360-372. doi:10.1016/j.tins.2018.03.006
- Huang, S., Ge, X., Yu, J., Han, Z., Yin, Z., Li, Y., Chen, F., Wang, H., Zhang, J. and Lei, P. (2018). Increased miR-124-3p in microglial exosomes following traumatic brain injury inhibits neuronal inflammation and contributes to neurite outgrowth via their transfer into neurons. *FASEB J.* **32**, 512-528. doi:10.1096/fj.201700673R
- Jessen, K. R. and Arthur-Farraj, P. (2019). Repair Schwann cell update: adaptive reprogramming, EMT, and stemness in regenerating nerves. *Glia* **67**, 421-437. doi:10.1002/glia.23532

- Jessen, K. R. and Mirsky, R. (2016). The repair Schwann cell and its function in regenerating nerves. *J. Physiol.* **594**, 3521–3531. doi:10.1113/JP270874
- Jessen, K. R. and Mirsky, R. (2019). The success and failure of the schwann cell response to nerve injury. *Front. Cell. Neurosci.* **13**, 33. doi:10.3389/fncel.2019.00033
- Jessen, K. R., Mirsky, R. and Arthur-Farraj, P. (2015). The role of cell plasticity in tissue repair: adaptive cellular reprogramming. *Dev. Cell* **34**, 613–620. doi:10.1016/j.devcel.2015.09.005
- Johnston, A. P., Yuzwa, S. A., Carr, M. J., Mahmud, N., Storer, M. A., Krause, M. P., Jones, K., Paul, S., Kaplan, D. R. and Miller, F. D. (2016). Dedifferentiated schwann cell precursors secreting paracrine factors are required for regeneration of the mammalian digit tip. *Cell Stem Cell* **19**, 433–448. doi:10.1016/j.stem.2016.06.002
- Kaselis, A., Treinys, R., Vosyliūtė, R. and Šatkauskas, S. (2014). DRG axon elongation and growth cone collapse rate induced by Sema3A are differently dependent on NGF concentration. *Cell. Mol. Neurobiol.* **34**, 289–296. doi:10.1007/s10571-013-0013-x
- La Shu, S., Yang, Y., Allen, C. L., Maguire, O., Minderman, H., Sen, A., Ciesielski, M. J., Collins, K. A., Bush, P. J., Singh, P. et al. (2018). Metabolic reprogramming of stromal fibroblasts by melanoma exosome microRNA favours a pre-metastatic microenvironment. *Sci. Rep.* **8**, 12905. doi:10.1038/s41598-018-31323-7
- Lai, C. P., Kim, E. Y., Badr, C. E., Weissleder, R., Mempel, T. R., Tannous, B. A. and Breakefield, X. O. (2015). Visualization and tracking of tumour extracellular vesicle delivery and RNA translation using multiplexed reporters. *Nat. Commun.* **6**, 7029. doi:10.1038/ncomms8029
- Lee, Y., Jeon, K., Lee, J.-T., Kim, S. and Kim, V. N. (2002). MicroRNA maturation: stepwise processing and subcellular localization. *EMBO J.* **21**, 4663–4670.
- Li, T., Wang, J., Wang, H., Yang, Y., Wang, S., Huang, N., Wang, F., Gao, X., Niu, J., Li, Z. et al. (2018). The deletion of *dicer* in mature myelinating glial cells causes progressive axonal degeneration but not overt demyelination in adult mice. *Glia* **66**, 1960–1971. doi:10.1002/glia.23450
- Liu, K., Lu, Y., Lee, J. K., Samara, R., Willenberg, R., Sears-Kraxberger, I., Tedeschi, A., Park, K. K., Jin, D., Cai, B. et al. (2010). PTEN deletion enhances the regenerative ability of adult corticospinal neurons. *Nat. Neurosci.* **13**, 1075–1081. doi:10.1038/nn.2603
- Lopez-Leal, R. and Court, F. A. (2016). Schwann cell exosomes mediate neuron–glia communication and enhance axonal regeneration. *Cell. Mol. Neurobiol.* **36**, 429–436. doi:10.1007/s10571-015-0314-3
- López-Leal, R., Diaz, P. and Court, F. A. (2018). In vitro analysis of the role of Schwann cells on axonal degeneration and regeneration using sensory neurons from dorsal root ganglia. *Methods Mol. Biol.* **1739**, 255–267. doi:10.1007/978-1-4939-7649-2_16
- Lopez-Verrilli, M. A. M. A., Picou, F. and Court, F. A. F. A. (2013). Schwann cell-derived exosomes enhance axonal regeneration in the peripheral nervous system. *Glia* **61**, 1795–1806. doi:10.1002/glia.22558
- Lorenz, R., Bernhart, S. H., Höner zu Siederdissen, C., Tafer, H., Flamm, C., Stadler, P. F. and Hofacker, I. L. (2011). ViennaRNA Package 2.0. *Algorithms Mol. Biol.* **6**, 26. doi:10.1186/1748-7188-6-26
- Love, M. I., Huber, W. and Anders, S. (2014). Moderated estimation of fold change and dispersion for RNA-seq data with DESeq2. *Genome Biol.* **15**, 550. doi:10.1186/s13059-014-0550-8
- Martini, R., Fischer, S., López-Vales, R. and David, S. (2008). Interactions between Schwann cells and macrophages in injury and inherited demyelinating disease. *Glia* **56**, 1566–1577. doi:10.1002/glia.20766
- McNamara, R. P., Chugh, P. E., Bailey, A., Costantini, L. M., Ma, Z., Bigi, R., Cheves, A., Eason, A. B., Landis, J. T., Host, K. M. et al. (2019). Extracellular vesicles from Kaposi Sarcoma-associated herpesvirus lymphoma induce long-term endothelial cell reprogramming. *PLoS Pathog.* **15**, e1007536. doi:10.1371/journal.ppat.1007536
- Mindos, T., Dun, X., North, K., Doddrell, R. D. S., Schulz, A., Edwards, P., Russell, J., Gray, B., Roberts, S. L., Shivane, A. et al. (2017). Merlin controls the repair capacity of Schwann cells after injury by regulating Hippo/YAP activity. *J. Cell Biol.* **216**, 495–510. doi:10.1083/jcb.201606052
- Monje, P. V., Rendon, S., Athauda, G., Bates, M., Wood, P. M. and Bunge, M. B. (2009). Non-antagonistic relationship between mitogenic factors and cAMP in adult Schwann cell re-differentiation. *Glia* **57**, 947–961. doi:10.1002/glia.20819
- Ohtake, Y., Hayat, U. and Li, S. (2015). PTEN inhibition and axon regeneration and neural repair. *Neural Regen. Res.* **10**, 1363–1368. doi:10.4103/1673-5374.165496
- Painter, M. W., Brosius Lutz, A., Cheng, Y.-C., Latremoliere, A., Duong, K., Miller, C. M., Posada, S., Cobos, E. J., Zhang, A. X., Wagers, A. J. et al. (2014). Diminished schwann cell repair responses underlie age-associated impaired axonal regeneration. *Neuron* **83**, 331–343. doi:10.1016/j.neuron.2014.06.016
- Park, K. K., Liu, K., Hu, Y., Smith, P. D., Wang, C., Cai, B., Xu, B., Connolly, L., Kramvis, I., Sahin, M. et al. (2008). Promoting axon regeneration in the adult CNS by modulation of the PTEN/mTOR pathway. *Science* **322**, 963–966. doi:10.1126/science.1161566
- Parkinson, D. B., Bhaskaran, A., Arthur-Farraj, P., Noon, L. A., Woodhoo, A., Lloyd, A. C., Feltri, M. L., Wrabetz, L., Behrens, A., Mirsky, R. et al. (2008). c-Jun is a negative regulator of myelination. *J. Cell Biol.* **181**, 625–637. doi:10.1083/jcb.200803013
- Ragusa, M., Barbagallo, C., Ciriigliaro, M., Battaglia, R., Brex, D., Caponnetto, A., Barbagallo, D., Di Pietro, C. and Purrello, M. (2017). Asymmetric RNA distribution among cells and their secreted exosomes: biomedical meaning and considerations on diagnostic applications. *Front. Mol. Biosci.* **4**, 66. doi:10.3389/fmolb.2017.00066
- Rajendran, L., Bali, J., Barr, M. M., Court, F. A., Krämer-Albers, E.-M., Picou, F., Raposo, G., Van Der Vos, K. E., Van Niel, G. and Wang, J. (2014). Emerging roles of extracellular vesicles in the nervous system. *J. Neurosci.* **34**, 15482–15489. doi:10.1523/JNEUROSCI.3258-14.2014
- Roberts, S. L., Dun, X., Doddrell, R. D. S., Mindos, T., Drake, L. K., Onaitis, M. W., Florio, F., Quattrini, A., Lloyd, A. C., D'Antonio, M. et al. (2017). Sox2 expression in Schwann cells inhibits myelination *in vivo* and induces influx of macrophages to the nerve. *Development* **144**, 3114–3125. doi:10.1242/dev.150656
- Santangelo, L., Giurato, G., Cicchini, C., Montaldo, C., Mancone, C., Tarallo, R., Battistelli, C., Alonzi, T., Weisz, A. and Tripodi, M. (2016). The RNA-binding protein SYNCRIP is a component of the hepatocyte exosomal machinery controlling MicroRNA sorting. *Cell Rep* **17**, 799–808. doi:10.1016/j.celrep.2016.09.031
- Schira, J., Heinen, A., Poschmann, G., Ziegler, B., Hartung, H. P., Stühler, K. and Küry, P. (2019). Secretome analysis of nerve repair mediating Schwann cells reveals Smad-dependent trophism. *FASEB J.* **33**, 4703–4715. doi:10.1096/fj.201801799R
- Schmieder, R. and Edwards, R. (2011). Quality control and preprocessing of metagenomic datasets. *Bioinformatics* **27**, 863–864. doi:10.1093/bioinformatics/btr026
- Shamash, S., Reichert, F. and Rotshenker, S. (2002). The cytokine network of Wallerian degeneration: tumor necrosis factor- α , interleukin-1 α , and interleukin-1 β . *J. Neurosci.* **22**, 3052–3060. doi:10.1523/JNEUROSCI.22-08-03052.2002
- Squadrito, M. L., Baer, C., Burdet, F., Maderna, C., Gilfillan, G. D., Lyle, R., Ibberson, M. and De Palma, M. (2014). Endogenous RNAs modulate MicroRNA sorting to exosomes and transfer to acceptor cells. *Cell Rep* **8**, 1432–1446. doi:10.1016/j.celrep.2014.07.035
- Steenbeek, S. C., Pham, T. V., de Ligt, J., Zomer, A., Knol, J. C., Piersma, S. R., Scheffhorst, T., Huisjes, R., Schifferers, R. M., Cuppen, E. et al. (2018). Cancer cells copy migratory behavior and exchange signaling networks via extracellular vesicles. *EMBO J.* **37**, e98357. doi:10.15252/embj.201798357
- Strickland, I. T., Richards, L., Holmes, F. E., Wynick, D., Uney, J. B. and Wong, L. F. (2011). Axotomy-induced mir-21 promotes axon growth in adult dorsal root ganglion neurons. *PLoS ONE* **6**, e23423. doi:10.1371/journal.pone.0023423
- Tassew, N. G., Charish, J., Shabanzadeh, A. P., Luga, V., Harada, H., Farhani, N., D'Onofrio, P., Choi, B., Ellabban, A., Nickerson, P. E. B. et al. (2017). Exosomes mediate mobilization of autocrine Wnt10b to promote axonal regeneration in the injured CNS. *Cell Rep* **20**, 99–111. doi:10.1016/j.celrep.2017.06.009
- Treiber, T., Treiber, N. and Meister, G. (2019). Regulation of microRNA biogenesis and its crosstalk with other cellular pathways. *Nat. Rev. Mol. Cell Biol.* **20**, 5–20. doi:10.1038/s41580-018-0059-1
- van Niel, G., D'Angelo, G. and Raposo, G. (2018). Shedding light on the cell biology of extracellular vesicles. *Nat. Rev. Mol. Cell Biol.* **19**, 213–228. doi:10.1038/nrm.2017.125
- Verrier, J. D., Semple-Rowland, S., Madorsky, I., Papin, J. E. and Notterpek, L. (2010). Reduction of *dicer* impairs Schwann cell differentiation and myelination. *J. Neurosci. Res.* **88**, 2558–2568. doi:10.1002/jnr.22418
- Viader, A., Chang, L. W., Fahrner, T., Nagarajan, R. and Milbrandt, J. (2011). MicroRNAs modulate schwann cell response to nerve injury by reinforcing transcriptional silencing of dedifferentiation-related genes. *J. Neurosci.* **31**, 17358–17369. doi:10.1523/JNEUROSCI.3931-11.2011
- Villarroya-Beltrí, C., Gutiérrez-Vázquez, C., Sánchez-Cabo, F., Pérez-Hernández, D., Vázquez, J., Martín-Cofreces, N., Martínez-Herrera, D. J., Pascual-Montano, A., Mittelbrunn, M. and Sánchez-Madrid, F. (2013). Sumoylated hnRNP A2B1 controls the sorting of miRNAs into exosomes through binding to specific motifs. *Nat. Commun.* **4**, 2980. doi:10.1038/ncomms3980
- Wang, J., Lu, M., Qiu, C. and Cui, Q. (2010). TransmiR: a transcription factor–microRNA regulation database. *Nucleic Acids Res.* **38**, D119–D122. doi:10.1093/nar/gkp803
- Wei, Z., Fan, B., Ding, H., Liu, Y., Tang, H., Pan, D., Shi, J., Zheng, P., Shi, H., Wu, H. et al. (2019). Proteomics analysis of Schwann cell-derived exosomes: a novel therapeutic strategy for central nervous system injury. *Mol. Cell. Biochem.* **457**, 51–59. doi:10.1007/s11010-019-03511-0
- Wood, M. D. and Mackinnon, S. E. (2015). Pathways regulating modality-specific axonal regeneration in peripheral nerve. *Exp. Neurol.* **265**, 171–175. doi:10.1016/j.expneurol.2015.02.001
- Zhang, B., Shen, L., Shi, H., Pan, Z., Wu, L., Yan, Y., Zhang, X., Mao, F., Qian, H. and Xu, W. (2016). Exosomes from human umbilical cord mesenchymal stem cells: identification, purification, and biological characteristics. *Stem Cells Int.* **2016**, 1929536. doi:10.1155/2016/1929536

- Zhou, J., Wang, K.-C., Wu, W., Subramaniam, S., Shyy, J. Y.-J., Chiu, J.-J., Li, J. Y.-S. and Chien, S. (2011). MicroRNA-21 targets peroxisome proliferators-activated receptor- α in an autoregulatory loop to modulate flow-induced endothelial inflammation. *Proc. Natl. Acad. Sci. USA* **108**, 10355-10360. doi:10.1073/pnas.1107052108
- Zochodne, D. W. (2012). The challenges and beauty of peripheral nerve regrowth. *J. Peripher. Nerv. Syst.* **17**, 1-18. doi:10.1111/j.1529-8027.2012.00378.x
- Zufferey, R., Nagy, D., Mandel, R. J., Naldini, L. and Trono, D. (1997). Multiply attenuated lentiviral vector achieves efficient gene delivery in vivo. *Nat. Biotechnol.* **15**, 871-875. doi:10.1038/nbt0997-871
- Zukor, K., Belin, S., Wang, C., Keelan, N., Wang, X. and He, Z. (2013). Short hairpin RNA against PTEN enhances regenerative growth of corticospinal tract axons after spinal cord injury. *J. Neurosci.* **33**, 15350-15361. doi:10.1523/jneurosci.2510-13.2013

Supplementary data

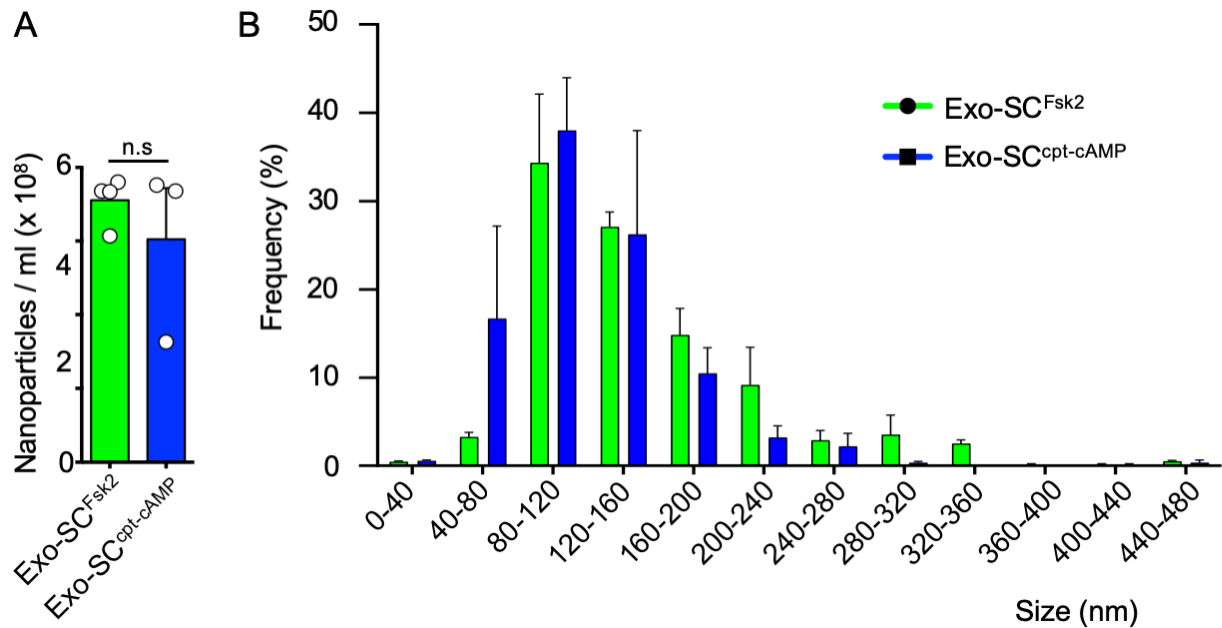


Figure S1. Quantitative comparison of exosomes derived from dSC and rSC. Schwann cell exosomes secreted by an equal number of 2 μ M forskolin (Fsk2) or 250 mM cpt-cAMP treated Schwann cells were characterized by nanosigth. **(A)** Density of exosomes derived from dSC and rSC. **(B)** Size profile of exosomes derived from dSC and rSC. n.s., non-significant by two tailed t-test.

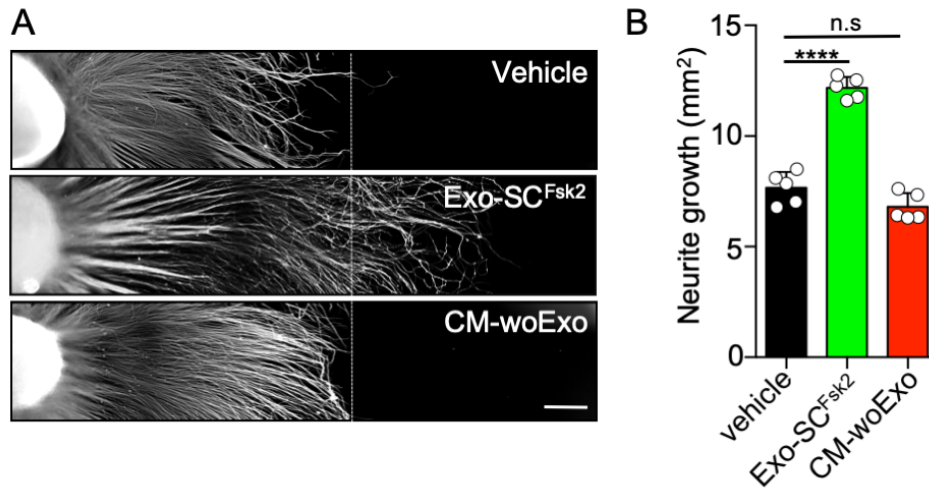


Figure S2. Neurite growth by rSC-exosomes versus rSC-conditioned medium (A) Neurite growth from DRG explants. Different treatments were daily administered per 3 days, including vehicle, exosomes from rSC (Exo-SC^{Fsk2}, 120 ng/ml) and rSC conditioned medium without exosomes (CM-woExo). After 3 days, DRG were visualized by acetylated tubulin immunostaining. Scale bar, 250 μ m. **(B)** Neurite growth area was quantified by measuring the neurite growth area minus explant body area. Mean neurite growth of DRG neurons \pm SEM, N=5; ****p<0.0001, n.s., non-significant by ANOVA test followed by Bonferroni post-test.

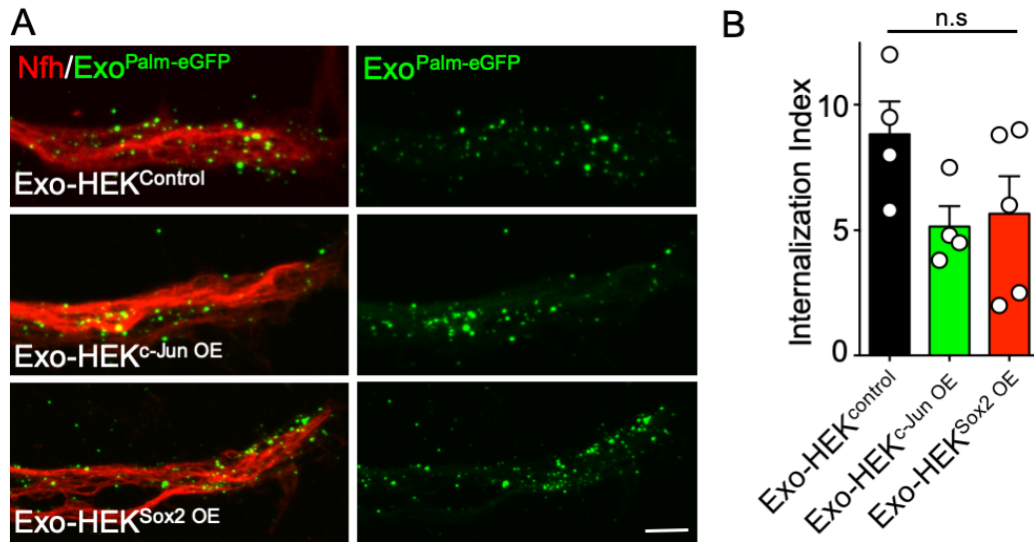


Figure S3. Internalization of HEK-derived exosomes by DRG neurons. (A) Exosomes were isolated from HEK cells transfected with CMV-Palm-eGFP to visualize exosomes and infected with pLenti-CMV-SOX2-P2A-GFP (NM_003106.3), pLenti-CMV-JUN-P2A-GFP (NM_002228) or an empty vector pLenti-CMV-Empty-P2A-GFP. DRG explants were treated with 5 μ g of exosome-eGFP for 3 hours, washed and immunostained against neurofilament heavy chain (Nfh, red) and eGFP (green). Scale bar, 2 μ m. (B) The internalization index was obtained from confocal images and deconvoluted z-stack images by measuring the eGFP mean staining area colocalized with the Nfh staining. Internalization index from 5 neurites from 4 separate experiments. n.s., non-significant by two tailed t-test.

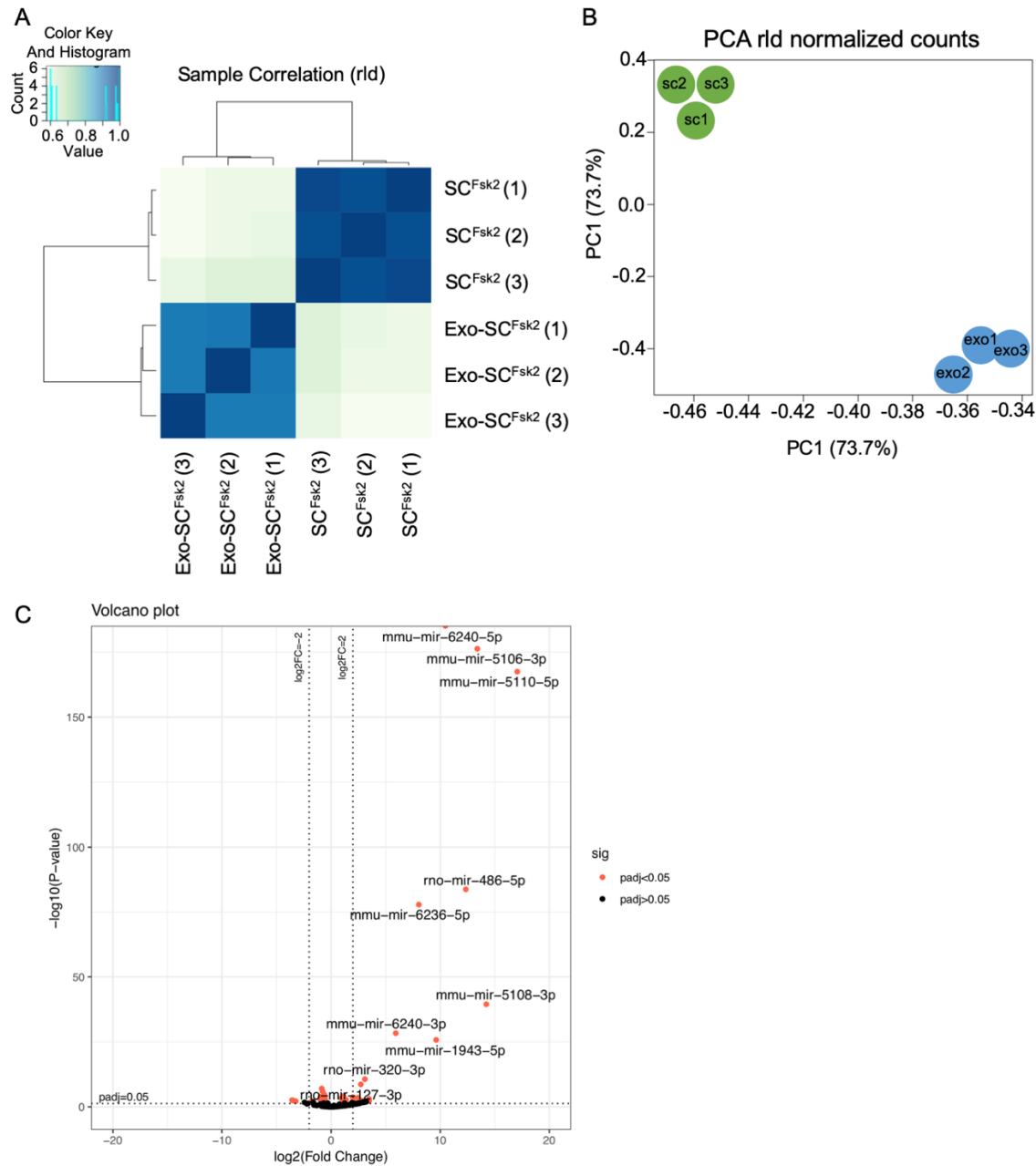


Figure S4. Small RNA-seq analysis of repair Schwann cells and their secreted exosomes. (A) Heat map of showing correlation between samples (Pearson's correlation coefficient) using expression levels of miRNAs. Sample labels Exo-SC are for exosomes and SC for Schwann cells. (B) Principal Component Analysis (PCA) of analyzed samples (Schwann cell samples in green and exosome samples in blue), indicating that miRNA expression was very different between samples (SC and exosomes). The percentage of variation in the data explained by the first and second principal component is indicated between brackets. (C) Volcano plot showing differentially expressed miRNAs from rSC exosomes compared to their cells of origin (rSC). Points are colored by significance. Genes with log₂FoldChange < 0 and padj < 0.05 were considered differentially expressed.

Cell type	Condition	Cell count	Conditioned media, CM (ml)	Protein amount in the exosome fraction from 10ml of CM (µg/ml)	Number of exosome particles in 12 ng
Schwann Cells	Fsk 2 µM	2×10^6	10	32.10 ± 7.48	$3.55 \times 10^8 \pm 3.55 \times 10^7$
	cpt-cAMP	2×10^6	10	18.24 ± 5.34	$3.16 \times 10^8 \pm 3.52 \times 10^7$
HEK overexpression	c-Jun	4×10^6	10	95.83 ± 27.11	$5.05 \times 10^8 \pm 3.67 \times 10^7$
	Sox2	4×10^6	10	125.44 ± 24.33	$4.39 \times 10^8 \pm 2.68 \times 10^7$
	Empty	4×10^6	10	131.15 ± 30.40	$6.89 \times 10^8 \pm 2.19 \times 10^7$

Table S1. Relationship between protein content and number of exosome particles per condition.

Exosomes isolated from 10 ml of conditioned medium from dSC, rSC, and HEK cells overexpressing c-Jun, Sox2 and empty vector were analyzed measuring protein amounts and the number of particles by nanosigth. After protein quantification by BCA method (described in the materials and methods section), exosomes were normalized to stock concentration of 12 ng/µl. The same preparations were analyzed by nanosigth to determine the particles concentration per volume.